Applied Mathematical Modelling 39 (2015) 7244–7265

Contents lists available at ScienceDirect

Applied Mathematical Modelling

journal homepage: www.elsevier.com/locate/apm

Seismic ground motion in micropolar elastic half-space

Maheshreddy Gade, S.T.G. Raghukanth *

Dept. of Civil Engineering, IIT Madras, India

ARTICLE INFO

Article history:
Received 6 May 2013
Received in revised form 14 February 2015
Accepted 5 March 2015
Available online 18 March 2015

Keywords:
Strong ground motion
Micro-rotations
Reduced micro polar continuum

ABSTRACT

In this article, analytic expressions for the frequency wave number spectra are derived for the displacement and rotational components at the ground surface of a micropolar elastic half-space. The ground motion is caused by buried sources described in terms of unit impulsive force and micro-moments. Closed-form analytic expressions for both plane strain and anti-plane strain conditions are established. In the sequel, Green's functions for reduced micro polar half-space where the couple stresses are zero and the stress tensor is nonsymmetric are also presented. Numerical results are presented for anti-plane strain case. The derived expressions can be used to simulate rotational and displacement components of ground motion during earthquakes.

1. Introduction

The dynamic response of an elastic half-space due to buried seismic sources has been a subject of great interest to seismologists and engineers for computing the surface ground motion. Beginning with the pioneering work of Lamb [1] on elastic waves generated by line sources, several articles on ground motion simulation in layered elastic media have appeared in the technical literature [2–6]. In these studies, analytical expressions for three translational components have been derived based on classical continuum mechanics theory. These analytical models are widely used for investigating the interior structure of the earth as well as earthquake source process through modeling of the recorded strong motion data [7,8].

On the other hand, studies on rotational components of ground motion and its effects on engineering structures are still not clear. The difficulty in measuring rotational components is mainly due to lack of technology in the strong motion devices to observe such small rotations in wide frequency band and distance range. However, there have been many reports about rotation of obelisks, grave stones and buildings during past earthquakes [9,10]. Many structural failures and much of the damage caused by earthquakes have been attributed to rotational ground motions [11]. There have been evidences during the past earthquakes and theoretical studies also show that contribution from rotational excitations reaches almost 50% of the total response. Recently, with modern acquisition technology such as fiber-optical or ring laser gyros, it has become possible to measure rotational motions during earthquakes. Takeo [12] recorded near-field rotational ground motion for several events during earthquake swarm in Izu peninsula, Japan. Igel et al. [13] and Suryanto et al. [14] obtained rotational time histories at teleseismic distances for M_w 8.1 Tokachi-Oki (2003) and M_w 6.3 Al Hoceima, Morocco earthquake (2004). There have been efforts in the past to develop mechanistic models for computing rotational time histories. Bouchon and Aki [15] simulated rotational ground motions in the near-field due to buried strike-slip and dip-slip faults in the layered medium. The rotational components induced by seismic waves are obtained from the space derivatives of the displacements.

* Corresponding author.
E-mail address: raghukanth@iitm.ac.in (S.T.G. Raghukanth).

http://dx.doi.org/10.1016/j.apm.2015.03.006
0307-904X/

The simulated rotations were small compared to the amplitude of the translational components. Takeo [12] simulated rotational ground motions based on the classical continuum mechanics and compared them with the recorded rotational velocities of M_w 5.7 magnitude earthquake in Izu peninsula, Japan. These results showed that the recorded rotations are several times larger than the simulated rotations computed from linear displacements. These differences have been attributed to the internal structure and discontinuities in the earth's crust. In order to get reliable estimates of rotations, one will have to model the microstructure of the medium itself as correctly as possible. In this regard, the linear theory of micropolar elasticity developed by Eringen [16] will be a suitable tool in simulating all the six components of ground motion. In the micropolar continuum theory, deformation is described not only by the displacement vector **u** but also by the rotation vector $\boldsymbol{\phi}$, which characterizes the micro-rotation of the particle. Kulesh et al. [17–19] and Grekova et al. [20] studied wave propagation in isotropic full and reduced Cosserat half-space. In this article, closed-form analytical expressions for the Green's functions in a two-dimensional micropolar medium are established. A spatial and temporal Fourier transform is used for solving the governing equations of motion. Analytical expressions are derived for the displacement and rotational components at the ground surface.

2. Basic equations of linear theory of micropolar elasticity

In continuum theories, a physical body B is considered to be a collection of a set of material particles. The motion of each material particle is described by a position vector identifying the location of each particle as a function of time. The number of degrees of freedom associated with each material point in classical continuum theory is three. In microcontinuum theories, it is assumed that there is a micro-structure around each material point which can deform and rotate independently from the surrounding medium [21]. The intrinsic deformation of a material particle is represented by a geometrical point and some deformable vectors, known as directors attached to the point that denotes the orientations and intrinsic deformations of the material particle. By increasing the number of directors attached to the material point, higher order microcontinuum theories can be derived. If the number of deformable directors is three, the material body is known as a micromorphic continuum. The number of degree of freedom associated with each material point in a micromorphic continuum is twelve. Assuming rigid directors, the degree of freedom at each material point reduces to six and the body is known as micropolar continuum. In the micropolar continuum theory, deformation is described by the displacement vector **u** and the rotation vector $\boldsymbol{\phi}$, which characterizes the micro-rotation of the particle [22]. The equations of motion for micropolar elastic solid are

$$\begin{aligned} &\sigma_{ji,j} + \rho X_i = \rho \ddot{u}_i, \\ &m_{ji,j} + \varepsilon_{ijk}\sigma_{jk} + \mathrm{J}Y_i = \mathrm{J}\ddot{\phi}_i, \end{aligned} \tag{1}$$

where σ_{ij}, m_{ij} are the stress and couple-stress tensors respectively. m_{ij} is the body force per unit mass and Y_i is the body couple per unit mass and ρ is the density of the medium. J is the parameter describing the rotational inertia of the medium. ε_{ijk} denotes the unit anti-symmetric tensor. The kinematic relations for infinitesimal strain (ϵ_{ij}) and curvature twist (φ_{ij}) tensor are expressed as

$$\begin{aligned} &\epsilon_{ij} = u_{j,i} + \varepsilon_{kji}\phi_k, \\ &\varphi_{ij} = \phi_{j,i}, \end{aligned} \tag{2}$$

The linear constitute laws for an isotropic micropolar elastic solid are

$$\begin{aligned} &\sigma_{ij} = \lambda \epsilon_{kk}\delta_{ij} + (\mu + \kappa)\epsilon_{ij} + \mu \epsilon_{ji}, \\ &m_{ij} = \alpha \varphi_{kk}\delta_{ij} + \beta \varphi_{ij} + \gamma \varphi_{ji}, \end{aligned} \tag{3}$$

where δ_{ij}, is the Kronecker delta, λ and μ are the Lame's constants respectively. α, β, γ and κ are the four new constants describing the microstructure medium. For internal energy to be a positive quantity, the six elastic constants has to satisfy the condition

$$\begin{aligned} &3\lambda + 2\mu + \kappa \geqslant 0, \quad \mu \geqslant 0, \quad \kappa \geqslant 0, \\ &3\alpha + \beta + \gamma \geqslant 0, \quad \gamma \geqslant \beta \geqslant 0, \quad \gamma \geqslant 0. \end{aligned} \tag{4}$$

By eliminating σ_{ij}, m_{ij}, φ_{ij} and ϵ_{ij} using Eqs. (2), (3) and (1), we obtain a system of six coupled equations of linear micropolar elasticity expressed in vector form as

$$\begin{aligned} &c_1^2 \nabla\nabla \cdot \boldsymbol{u} - c_2^2 \nabla \times \nabla \times \mathbf{u} + \frac{\mathrm{J}w_0^2}{2} \nabla \times \boldsymbol{\phi} - \ddot{\mathbf{u}} = 0, \\ &c_3^2 \nabla\nabla \cdot \boldsymbol{\phi} - c_4^2 \nabla \times \nabla \times \boldsymbol{\phi} + \frac{w_0^2}{2} \nabla \times \mathbf{u} - w_0^2 \boldsymbol{\phi} - \ddot{\boldsymbol{\phi}} = 0, \end{aligned} \tag{5}$$

where c_1, c_2, c_3, c_4 are the wave velocities

$$c_1^2 = \frac{\lambda + 2\mu + \kappa}{\rho}; \quad c_2^2 = \frac{\mu + \kappa}{\rho}; \quad c_3^2 = \frac{\alpha + \beta + \gamma}{\rho J}; \quad c_4^2 = \frac{\gamma}{\rho J}; \quad w_o^2 = \frac{2\kappa}{\rho J}. \tag{6}$$

It can be observed that, when $\kappa = 0$ the governing equations for displacement and microrotation become uncoupled. In this case, Eq. (5a) reduces to the displacement equations of motion of the classical elasticity. Eq. (5b) represents a hypothetical body in which only rotations occur.

3. Plane waves in an infinite micropolar elastic solid

In classical elasticity, two types of waves namely longitudinal and shear waves exist in an infinite medium. In micropolar theory, the microstructure of the medium reveals new types of waves not encountered in the classical continuum mechanics. According to Helmholtz decomposition, the field equations (Eq. (5)) in a micropolar elastic medium can be simplified by separating the displacement and microrotation components into potential and solenoidal parts in the following form

$$\mathbf{u} = \nabla q + \nabla \times \mathbf{\Psi}, \quad \nabla \cdot \mathbf{\Psi} = 0, \tag{7}$$

$$\boldsymbol{\phi} = \nabla \xi + \nabla \times \mathbf{\Phi}, \quad \nabla . \mathbf{\Phi} = 0. \tag{8}$$

By substituting the above equation in Eq. (5) and in absence of body forces and couples we obtain the following system of equations

$$c_1^2 \nabla^2 q - \ddot{q} = 0, \tag{9}$$

$$c_3^2 \nabla^2 \xi - w_0^2 \xi - \ddot{\xi} = 0, \tag{10}$$

$$c_2^2 \nabla^2 \mathbf{\Psi} + \frac{J w_0^2}{2} \nabla \times \mathbf{\Phi} - \ddot{\mathbf{\Psi}} = 0, \tag{11}$$

$$c_4^2 \nabla^2 \mathbf{\Phi} - w_0^2 \mathbf{\Phi} + \frac{w_0^2}{2} \nabla \times \mathbf{\Psi} - \ddot{\mathbf{\Phi}} = 0. \tag{12}$$

It can be observed that the equations for vector potentials $\mathbf{\Psi}$ and $\mathbf{\Phi}$ are coupled. Following Parfitt and Eringen [23], the plane waves advancing in the positive direction can be expressed as

$$\{q, \xi, \mathbf{\Psi}, \mathbf{\Phi}\} = \{\mathrm{a}, \mathrm{b}, \mathbf{A}, \mathbf{B}\} \exp[ik(\mathbf{n} \cdot \mathbf{r} - vt)], \tag{13}$$

where a, b are complex constants. **A, B** are complex constant vectors, k is the wave number, v is the phase velocity and $\mathbf{n}$ is the unit normal vector. Substituting q from Eq. (13) in Eq. (9) and using Eq. (7), the displacement vector can be obtained as

$$\boldsymbol{u} = ik_1 a \boldsymbol{n} \exp[ik_1(\mathbf{n} \cdot \mathbf{r} - v_1 t)], \tag{14}$$

where

$$v_1^2 = \frac{\lambda + 2\mu + \kappa}{\rho}. \tag{15}$$

It can be noted from Eq. (14) that the displacement of the particles is in the same direction as that of waves traveling at velocity v_1. Such a motion represents a train of longitudinal waves. These waves are similar to the dilatational waves encountered in the classical continuum mechanics. Similarly substituting the expression for ξ from Eq. (13) in Eqs. (10) and (8) yields

$$\phi = \nabla \xi = ik_2 b \boldsymbol{n} \exp[ik_2(\boldsymbol{n} \cdot \boldsymbol{r} - v_2 t)], \tag{16}$$

where the velocity of these waves can be expressed as

$$v_2^2 = \frac{\alpha + \beta + \gamma}{\rho J \left(1 - \frac{2\kappa}{\rho J \omega^2}\right)}. \tag{17}$$

It can be observed from Eq. (16) that the microrotation vector points in the direction of propagation of waves. These new dispersive waves are known as longitudinal microrotation waves. The speed (v_2) of these waves depend on frequency and are not encountered in the classical theory. Similarly Eqs. (13), (11) and (12) yield

$$(\omega^2 - c_2^2 k^2)\mathbf{A} + i\frac{J w_0^2}{2} \mathbf{n} \times \mathbf{B} = 0, \tag{18}$$

$$\frac{J w_0^2}{2} \boldsymbol{n} \times \mathbf{A} + (\omega^2 - w_0^2 - c_4^2)\mathbf{B} = 0. \tag{19}$$

Solving Eq. (19) for $\mathbf{B}$ gives

$$\mathbf{B} = \frac{-J w_0^2}{2(\omega^2 - w_0^2 - c_4^2)} \mathbf{n} \times \mathbf{A}. \tag{20}$$

The above equation indicates that the three vectors **n, A** and **B** are mutually perpendicular to each other. The waves associated with $\boldsymbol{\Psi}$ are known as transverse displacement waves and those waves associated with $\boldsymbol{\Phi}$ are known as transverse microrotation waves. By eliminating A and B from the above equations and solving for velocities of the coupled waves, we get

$$v_{3,4}^2 = \frac{w_0^2}{2k^2} + \frac{c_2^2 + c_4^2}{2} \pm \sqrt{\frac{1}{4}\left(\frac{w_0^2}{k^2} + c_4^2 - c_2^2\right)^2 + \frac{Jw_0^4}{4k^2}}. \tag{21}$$

The upper sign (+) corresponds to the velocity v_3 of the coupled transverse displacement wave and the lower sign (−) corresponds to the velocity v_4 of the coupled transverse microrotational waves. The coupled transverse displacement waves represent the counterpart of the classical shear waves and reduces to them when κ and γ are zero. The coupled transverse microrotational waves are new and are not encountered in the classical theory. The above expressions can be find in Eringen [24].

4. Ground motion at free surface of half-space due to a buried sources

Consider a homogeneous micropolar elastic half-space with free surface $y = 0$ and assume the wave normal **n** to lie in the xy-plane. The particle motion is invariant with respect to z if the wave normal is in xy-plane. Then, the displacements **u** and microrotations $\boldsymbol{\phi}$ are functions of x, y and t. The derivative with respective to z is zero. Subsequently, the six coupled equations (Eq. (5)) can be written as.

$$\begin{aligned}
&C_1^2\left[\frac{\partial^2 u_x}{\partial x^2} + \frac{\partial^2 u_y}{\partial x \partial y}\right] - C_2^2\left[\frac{\partial^2 u_y}{\partial x \partial y} - \frac{\partial^2 u_x}{\partial y^2}\right] + \frac{Jw_0^2}{2}\frac{\partial \phi_z}{\partial y} - \frac{\partial^2 u_x}{\partial t^2} = 0,\\
&C_1^2\left[\frac{\partial^2 u_x}{\partial x \partial y} + \frac{\partial^2 u_y}{\partial y^2}\right] + C_2^2\left[\frac{\partial^2 u_y}{\partial x^2} - \frac{\partial^2 u_x}{\partial x \partial y}\right] - \frac{Jw_0^2}{2}\frac{\partial \phi_z}{\partial x} - \frac{\partial^2 u_y}{\partial t^2} = 0,\\
&C_4^2\left[\frac{\partial^2 \phi_z}{\partial x^2} + \frac{\partial^2 \phi_z}{\partial y^2}\right] + \frac{w_0^2}{2}\left[\frac{\partial u_y}{\partial x} - \frac{\partial u_x}{\partial y}\right] - w_0^2\phi_z - \frac{\partial^2 \phi_z}{\partial t^2} = 0,\\
&C_3^2\left[\frac{\partial^2 \phi_x}{\partial x^2} + \frac{\partial^2 \phi_y}{\partial x \partial y}\right] - C_4^2\left[\frac{\partial^2 \phi_y}{\partial x \partial y} - \frac{\partial^2 \phi_x}{\partial y^2}\right] + \frac{w_0^2}{2}\frac{\partial u_z}{\partial y} - w_0^2\phi_x - \frac{\partial^2 \phi_x}{\partial t^2} = 0,\\
&C_3^2\left[\frac{\partial^2 \phi_x}{\partial x \partial y} + \frac{\partial^2 \phi_y}{\partial y^2}\right] + C_4^2\left[\frac{\partial^2 \phi_y}{\partial x^2} - \frac{\partial^2 \phi_x}{\partial x \partial y}\right] - \frac{w_0^2}{2}\frac{\partial u_z}{\partial x} - w_0^2\phi_y - \frac{\partial^2 \phi_y}{\partial t^2} = 0,\\
&C_2^2\left[\frac{\partial^2 u_z}{\partial x^2} + \frac{\partial^2 u_z}{\partial y^2}\right] + \frac{Jw_0^2}{2}\left[\frac{\partial \phi_y}{\partial x} - \frac{\partial \phi_x}{\partial y}\right] - \frac{\partial^2 u_z}{\partial t^2} = 0.
\end{aligned} \tag{22}$$

It can be observed that, two displacement components u_x, u_y and one microrotation component ϕ_z are coupled through Eqs. (22)(a–c). Eqs. 22(d–f) represents coupled equations for two microrotations ϕ_x, ϕ_y and one displacement component u_z. Further, from Eq. (3) it can be shown that the stresses σ_{xx}, σ_{yy}, σ_{xy}, σ_{yx}, m_{xz}, m_{yz}, m_{zx} and m_{zy} depend only on u_x, u_y and ϕ_z and the stresses σ_{xz}, σ_{yz}, σ_{zy}, σ_{zx}, m_{xx}, m_{yy}, m_{yx} and m_{xy} are functions of ϕ_x, ϕ_y and u_z. This makes it possible to resolve the 3D problem into two parts, where one is plane strain case corresponding to u_x, u_y and ϕ_z and the other is anti-plane strain case corresponding to ϕ_x, ϕ_y and u_z.

4.1. Plane strain

The Cartesian coordinates x and z are directed along the surface of the half-space and the y-axis is perpendicular to it. The solution to the buried source can be treated effectively as a half-space problem involving stress discontinuities across the plane $y = y_0$. For this purpose it is convenient to view the half-space as being composed of an upper and lower region of the same material defined as.

(I) Region I, $|x| < \infty, \quad 0 < y \leqslant y_0,$

(II) Region II, $|x| < \infty, \quad y_0 < y \leqslant \infty.$

For a plane strain problem, the displacement and rotation vector is represented as $\mathbf{u} = (u_x, u_y, 0)$ and $\phi = (0, 0, \phi_z)$. Two potential functions, q and $\boldsymbol{\Psi}$, can be defined to describe the displacements in x- and y-directions.

$$u_x = \frac{\partial q}{\partial x} + \frac{\partial \Psi}{\partial y}, \quad u_y = \frac{\partial q}{\partial y} - \frac{\partial \Psi}{\partial x}, \quad \phi_z = \phi. \tag{23}$$

The equations of motion for plane deformation parallel to *xy* plane in terms of the potentials are

$$\begin{aligned} &c_1^2\left(\frac{\partial^2 q}{\partial x^2}+\frac{\partial^2 q}{\partial y^2}\right)-\frac{\partial^2 q}{\partial t^2}=0,\\ &c_2^2\left(\frac{\partial^2 \Psi}{\partial x^2}+\frac{\partial^2 \Psi}{\partial y^2}\right)+\frac{Jw_0^2}{2}\phi-\frac{\partial^2 \Psi}{\partial t^2}=0,\\ &c_4^2\left(\frac{\partial^2 \phi}{\partial x^2}+\frac{\partial^2 \phi}{\partial y^2}\right)-w_0^2\phi-\frac{w_0^2}{2}\left(\frac{\partial^2 \Psi}{\partial x^2}+\frac{\partial^2 \Psi}{\partial y^2}\right)-\frac{\partial^2 \phi}{\partial t^2}=0. \end{aligned} \tag{24}$$

The constitutive equations (Eq. (3)) in terms of potentials can be written as

$$\begin{aligned} &\sigma_{xx}=\lambda\nabla^2 q+(2\mu+\kappa)\left(\frac{\partial^2 q}{\partial x^2}+\frac{\partial^2 \Psi}{\partial x\partial y}\right),\\ &\sigma_{yy}=\lambda\nabla^2 q+(2\mu+\kappa)\left(\frac{\partial^2 q}{\partial y^2}-\frac{\partial^2 \Psi}{\partial x\partial y}\right),\\ &\sigma_{xy}=(2\mu+\kappa)\frac{\partial^2 \mathrm{q}}{\partial x\partial y}+\mu\frac{\partial^2 \Psi}{\partial y^2}-(\mu+\kappa)\frac{\partial^2 \Psi}{\partial x^2}-\kappa\phi,\\ &\sigma_{yx}=(2\mu+\kappa)\frac{\partial^2 \mathrm{q}}{\partial x\partial y}-\mu\frac{\partial^2 \Psi}{\partial x^2}+(\mu+\kappa)\frac{\partial^2 \Psi}{\partial y^2}+\kappa\phi,\\ &m_{xz}=\beta\frac{\partial\phi}{\partial x},\quad m_{yz}=\beta\frac{\partial\phi}{\partial y},\quad m_{zx}=\gamma\frac{\partial\phi}{\partial x},\quad m_{zy}=\gamma\frac{\partial\phi}{\partial y}. \end{aligned} \tag{25}$$

The buried sources inside the medium can be effectively treated as stress discontinuities across the plane $y = y_0$. The three loading cases considered in this study are shown in Fig. 1(a)–(c). The magnitude of these three loads acting on the line $y = y_0$ are $\exp[-i(kx + \omega t)]$ per unit length. These can be expressed as

$$\sigma_{yy}(x,y=y_0^+,t)-\sigma_{yy}(x,y=y_0^-,t)=\exp[-i(kx+\omega t)], \tag{26}$$

$$\sigma_{yx}(x,y=y_0^+,t)-\sigma_{yx}(x,y=y_0^-,t)=\exp[-i(kx+\omega t)], \tag{27}$$

$$m_{yz}(x,y=y_0^+,t)-m_{yz}(x,y=y_0^-,t)=\exp[-i(kx+\omega t)]. \tag{28}$$

The displacements and micro-rotations are required to be continuous across the plane $y = y_0$. These are given as

$$u_x(x,y=y_0^+,t)=u_x(x,y=y_0^-,t), \tag{29}$$

$$u_y(x,y=y_0^+,t)=u_y(x,y=y_0^-,t), \tag{30}$$

$$\phi(x,y=y_0^+,t)=\phi(x,y=y_0^-,t), \tag{31}$$

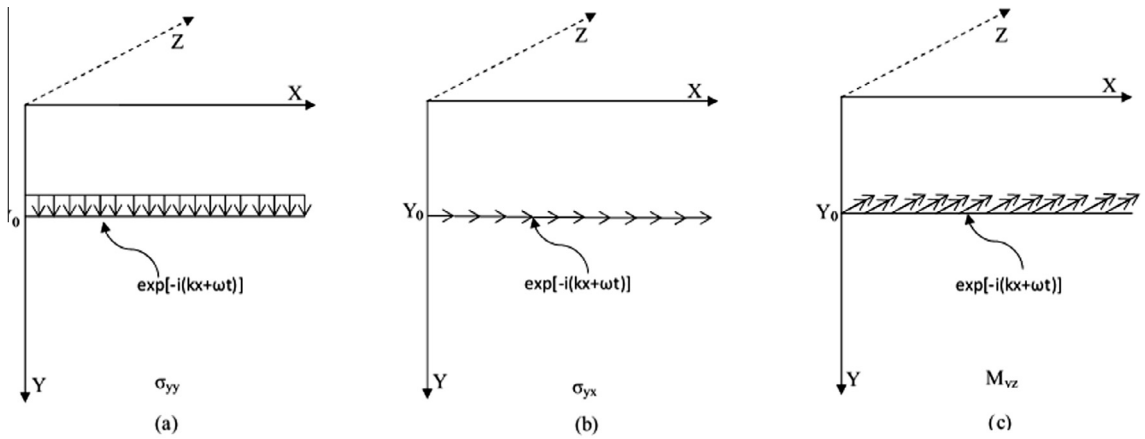

Fig. 1. (a)–(c) Three loading conditions for plane strain problem.

The boundary conditions in a half-space are given by the vanishing of stresses at the free surface which is

$$\sigma_{yy}(x,0,t) = \sigma_{yx}(x,0,t) = m_{yz}(x,0,t) = 0. \tag{32}$$

The solutions of Eq. (24) can be written as

$$\begin{aligned} q(x,y,t) &= \tilde{q}(y)\exp[-i(kx+\omega t)],\\ \Psi(x,y,t) &= \tilde{\Psi}(y)\exp[-i(kx+\omega t)],\\ \phi(x,y,t) &= \tilde{\phi}(y)\exp[-i(kx+\omega t)]. \end{aligned} \tag{33}$$

Here k is the real wave number along the x direction and ω stands for frequency. Substituting the above equation in Eq. (24), the governing equations can be rewritten as

$$\begin{aligned} &\frac{d^2\tilde{q}}{dy^2} + \left(\frac{\omega^2}{c_1^2} - k^2\right)\tilde{q} = 0,\\ &\frac{d^2\tilde{\Psi}}{dy^2} + \left(\frac{\omega^2}{c_2^2} - k^2\right)\tilde{\Psi} + \mathrm{J}\frac{w_0^2}{2c_2^2}\tilde{\phi} = 0,\\ &\frac{d^2\tilde{\phi}}{dy^2} + \left(\frac{\omega^2}{c_4^2} - \frac{w_0^2}{c_4^2} - k^2\right)\tilde{\phi} - \frac{w_0^2}{2c_4^2}\frac{d^2\tilde{\Psi}}{dy^2} + \frac{k^2 w_0^2}{2c_4^2}\tilde{\Psi} = 0. \end{aligned} \tag{34}$$

In region I, the solution to the equation can be expressed as

$$\begin{aligned} \tilde{q}(y) &= A^{\mathrm{I}}e^{-i\nu_0(y-y_0)} + B^{\mathrm{I}}e^{i\nu_0(y-y_0)},\\ \tilde{\Psi}(y) &= D_1^{\mathrm{I}}e^{-i\nu_1(y-y_0)} + D_2^{\mathrm{I}}e^{-i\nu_2(y-y_0)} + D_3^{\mathrm{I}}e^{i\nu_1(y-y_0)} + D_4^{\mathrm{I}}e^{i\nu_2(y-y_0)},\\ \tilde{\phi}(y) &= \vartheta_1\left(D_1^{\mathrm{I}}e^{-i\nu_1(y-y_0)} + D_3^{\mathrm{I}}e^{i\nu_1(y-y_0)}\right) + \vartheta_2\left(D_2^{\mathrm{I}}e^{-i\nu_2(y-y_0)} + D_4^{\mathrm{I}}e^{i\nu_2(y-y_0)}\right). \end{aligned} \tag{35}$$

In region II and below the seismic source

$$\begin{aligned} \tilde{q}(y) &= A^{\mathrm{II}}e^{-i\nu_0(y-y_0)},\\ \tilde{\Psi}(y) &= D_1^{\mathrm{II}}e^{-i\nu_1(y-y_0)} + D_2^{\mathrm{II}}e^{-i\nu_2(y-y_0)},\\ \tilde{\phi}(y) &= \vartheta_1\left(D_1^{\mathrm{II}}e^{-i\nu_1(y-y_0)}\right) + \vartheta_2\left(D_2^{\mathrm{II}}e^{-i\nu_2(y-y_0)}\right), \end{aligned} \tag{36}$$

where

$$\vartheta_1 = \frac{2c_2^2}{\mathrm{J}w_0^2}\left(k^2 + \nu_1^2 - \frac{\omega^2}{c_2^2}\right),$$

$$\vartheta_2 = \frac{2c_2^2}{\mathrm{J}w_0^2}\left(k^2 + \nu_2^2 - \frac{\omega^2}{c_2^2}\right).$$

ν_0, ν_1 and ν_2 are the vertical wave numbers defined through,

$$\begin{aligned} &\nu_0 = \sqrt{\frac{\omega^2}{c_1^2} - k^2}, \quad \nu_1 = \sqrt{a_1 - k^2}, \quad \nu_2 = \sqrt{a_2 - k^2},\\ &a_{1,2} = \frac{(c_2^2 + c_4^2)\omega^2}{2c_2^2c_4^2} + \frac{(w_0^2\mathrm{J} - 4c_2^2)w_0^2}{8c_2^2c_4^2} \pm \sqrt{\frac{(c_2^2 - c_4^2)^2}{4c_2^4c_4^4}\omega^4 + \frac{w_0^2(w_0^2\mathrm{J}(c_2^2 + c_4^2) - 4c_2^2(c_2^2 - c_4^2))}{8c_2^4c_4^4}\omega^2 + \frac{w_0^4(w_0^2\mathrm{J} - 4c_2^2)^2}{64c_2^4c_4^4}}. \end{aligned} \tag{37}$$

The total numbers of unknown coefficients are 9. These constants have to be found from the above nine boundary conditions. The stress free boundary condition on the surface of the half-space (Eq. (32)) results in

$$D_2^{\mathrm{I}} = \frac{1}{\Gamma_5 + \Gamma_2\Gamma_3 - \Gamma_1\Gamma_4}\left[(2k\nu_0\mathrm{J}w_0^2(2\mu+\kappa)\Gamma_3e^{-iy_0(\nu_2+\nu_0)})B^{\mathrm{I}} - (2\Gamma_1\Gamma_3e^{-iy_0(\nu_1+\nu_2)})D_3^{\mathrm{I}} - ((\Gamma_1\Gamma_4 - \Gamma_5 + \Gamma_2\Gamma_3)e^{-2i\nu_2y_0})D_4^{\mathrm{I}}\right], \tag{38}$$

$$D_1^{\mathrm{I}} = e^{-2i\nu_1y_0}D_3^{\mathrm{I}} + \frac{\Gamma_6}{\Gamma_7}\left(e^{-iy_0(\nu_1+\nu_2)}D_4^{\mathrm{I}} - e^{iy_0(\nu_{2-}\nu_1)}D_2^{\mathrm{I}}\right), \tag{39}$$

$$A^{\mathrm{I}} = -e^{-2i\nu_0y_0}B^{\mathrm{I}} + \frac{\Gamma_8}{\Gamma_9}\left(e^{iy_0(\nu_{2-}\nu_0)}D_2^{\mathrm{I}} - e^{-iy_0(\nu_0+\nu_2)}D_4^{\mathrm{I}}\right). \tag{40}$$

From the continuity of displacements and rotations along the plane $y = y_0$ (Eqs. (29)–(31)), the constants A^{II}, D_1^{II} and D_2^{II} can be expressed as

$$A^{II} = A^{I} + \frac{\Gamma_{10}B^{I} - 2kc_2^2(v_1+v_2)\left(v_1D_3^{I} + v_2D_4^{I}\right)}{\Gamma_{11}}, \tag{41}$$

$$D_1^{II} = D_1^{I} + \frac{2v_0\left(\omega^2 - c_2^2(k^2+v_2^2)\right)\left(kB^{I} - v_2D_4^{I}\right) + (v_1+v_2)\Gamma_{12}D_3^{I}}{(v_1-v_2)\Gamma_{11}}, \tag{42}$$

$$D_2^{II} = D_2^{I} - \frac{2v_0\left(\omega^2 - c_2^2(k^2+v_1^2)\right)\left(kB^{I} - v_1D_3^{I}\right) - (v_1+v_2)\Gamma_{13}D_4^{I}}{(v_1-v_2)\Gamma_{11}}, \tag{43}$$

where

$$\Gamma_1 = Jw_0^2\left(\mu k^2 - v_1^2(\mu+\kappa)\right) - 2\kappa\left(\omega^2 - c_2^2(k^2+v_1^2)\right),$$

$$\Gamma_2 = Jw_0^2\left(\mu k^2 - v_2^2(\mu+\kappa)\right) - 2\kappa\left(\omega^2 - c_2^2(k^2+v_2^2)\right),$$

$$\Gamma_3 = v_1\left(c_2^2(k^2+v_1^2) - \omega^2\right)\left(\lambda(k^2+v_0^2) + v_0^2(2\mu+\kappa)\right),$$

$$\Gamma_4 = v_2\left(c_2^2(k^2+v_2^2) - \omega^2\right)\left(\lambda(k^2+v_0^2) + v_0^2(2\mu+\kappa)\right),$$

$$\Gamma_5 = k^2c_2^2Jw_0^2v_0v_1v_2(v_1^2 - v_2^2)(2\mu+\kappa)^2,$$

$$\Gamma_6 = v_2\left(c_2^2(k^2+v_2^2) - \omega^2\right),$$

$$\Gamma_7 = v_1\left(c_2^2(k^2+v_1^2) - \omega^2\right),$$

$$\Gamma_8 = kv_2c_2^2(v_1^2 - v_2^2)(2\mu+\kappa),$$

$$\Gamma_9 = \left(c_2^2(k^2+v_1^2) - \omega^2\right)\left(\lambda(k^2+v_0^2) + v_0^2(2\mu+\kappa)\right),$$

$$\Gamma_{10} = \kappa^2c_2^2(v_1+v_2) - v_0\left(\omega^2 - c_2^2(k^2 - v_1v_2)\right),$$

$$\Gamma_{11} = \kappa^2c_2^2(v_1+v_2) + v_0\left(\omega^2 - c_2^2(k^2 - v_1v_2)\right),$$

$$\Gamma_{12} = \kappa^2c_2^2(v_1-v_2) - v_0\left(\omega^2 - c_2^2(k^2 + v_1v_2)\right),$$

$$\Gamma_{13} = \kappa^2c_2^2(v_1-v_2) + v_0(\omega^2 - c_2^2(k^2 + v_1v_2)).$$

Six coefficients $\left(A^{I},\ D_1^{I},\ D_2^{I},\ A^{II},\ D_1^{II}\right.$ and $\left.D_2^{II}\right)$ are expressed in terms of other three coefficients $\left(B^{I}, D_3^{I},\right.$ and $\left.D_4^{I}\right)$ in above equations (Eqs. (38)–(43)). These three coefficients have to be estimated by using stress discontinuity boundary condition along the plane $y = y_0$ (Eqs. (26)–(28)).

4.1.1. Results for specific source distributions

Loading case I:

$$\tilde{\sigma}_{yy}(x, y = y_0^+, t) - \tilde{\sigma}_{yy}(x, y = y_0^-, t) = 0,$$

$$\tilde{\sigma}_{yx}(x, y = y_0^+, t) - \tilde{\sigma}_{yx}(x, y = y_0^-, t) = \exp[-i(kx + \omega t)],$$

$$\tilde{m}_{yz}(x, y = y_0^+, t) - \tilde{m}_{yz}(x, y = y_0^-, t) = 0,$$

$$B^{I} = \frac{-kc_2^2}{2v_0\omega^2(\mu+\kappa)}, \tag{44}$$

$$D_3^{\mathrm{I}} = -\frac{(c_2^2(k^2+v_2^2)-\omega^2)}{2\omega^2(\mu+\kappa)(v_1^2-v_2^2)}, \tag{45}$$

$$D_4^{\mathrm{I}} = \frac{(c_2^2(k^2+v_1^2)-\omega^2)}{2\omega^2(\mu+\kappa)(v_1^2-v_2^2)}, \tag{46}$$

Loading case II:

$$\tilde{\sigma}_{yy}(x,y=y_0^+,t) - \tilde{\sigma}_{yy}(x,y=y_0^-,t) = \exp[-i(kx+\omega t)],$$

$$\tilde{\sigma}_{yx}(x,y=y_0^+,t) - \tilde{\sigma}_{yx}(x,y=y_0^-,t) = 0,$$

$$\tilde{m}_{yz}(x,y=y_0^+,t) - \tilde{m}_{yz}(x,y=y_0^-,t) = 0$$

$$B^{\mathrm{I}} = \frac{1}{2(\lambda+2\mu+\kappa)(k^2+v_0^2)}, \tag{47}$$

$$D_3^{\mathrm{I}} = -\frac{k(c_2^2(k^2+v_2^2)-\omega^2)}{2c_2^2 v_1(\lambda+2\mu+\kappa)(v_1^2-v_2^2)}, \tag{48}$$

$$D_4^{\mathrm{I}} = \frac{k(c_2^2(k^2+v_1^2)-\omega^2)}{2c_2^2 v_2(\lambda+2\mu+\kappa)(v_1^2-v_2^2)}. \tag{49}$$

Loading case III:

$$\tilde{\sigma}_{yy}(x,y=y_0^+,t) - \tilde{\sigma}_{yy}(x,y=y_0^-,t) = 0,$$

$$\tilde{\sigma}_{yx}(x,y=y_0^+,t) - \tilde{\sigma}_{yx}(x,y=y_0^-,t) = 0,$$

$$\tilde{m}_{yz}(x,y=y_0^+,t) - \tilde{m}_{yz}(x,y=y_0^-,t) = \exp[-i(kx+\omega t)],$$

$$B^{\mathrm{I}} = 0, \tag{50}$$

$$D_3^{\mathrm{I}} = \frac{i\mathrm{J}w_0^2}{4c_2^2 v_1\beta(v_1^2-v_2^2)}, \tag{51}$$

$$D_4^{\mathrm{I}} = -\frac{i\mathrm{J}w_0^2}{4c_2^2 v_2\beta(v_1^2-v_2^2)}. \tag{52}$$

The obtained solutions are valid for the loading cases shown in Fig. 1 where the loads act periodically all over the plane $y = y_0$ and harmonically in time. The corresponding solutions for the three unidirectional unit impulses can be obtained by using the Fourier integral representation of the Dirac delta function.

4.2. Anti-plane strain

For a anti-plane strain problem, the displacement and rotation vector is represented as $\mathbf{u} = (0,0,u_z)$ and $\phi = (\phi_x,\phi_y,0)$. Two potential functions, ξ and Φ can be defined to describe the rotations about x- and y-directions.

$$\phi_x = \frac{\partial\xi}{\partial x} + \frac{\partial\Phi}{\partial y}, \quad \phi_y = \frac{\partial\xi}{\partial y} - \frac{\partial\Phi}{\partial x}, \quad u_z = u_z. \tag{53}$$

The equations of motion for plane deformation parallel to xy plane in terms of the potentials are

$$\begin{aligned} c_3^2\left(\frac{\partial^2\xi}{\partial x^2}+\frac{\partial^2\xi}{\partial y^2}\right) - w_0^2\xi - \frac{\partial^2 q}{\partial t^2} &= 0,\\ c_2^2\left(\frac{\partial^2 u_z}{\partial x^2}+\frac{\partial^2 u_z}{\partial y^2}\right) - \frac{\mathrm{J}w_0^2}{2}\left(\frac{\partial^2\Phi}{\partial x^2}+\frac{\partial^2\Phi}{\partial y^2}\right) - \frac{\partial^2 u_z}{\partial t^2} &= 0,\\ c_4^2\left(\frac{\partial^2\Phi}{\partial x^2}+\frac{\partial^2\Phi}{\partial y^2}\right) - w_0^2\Phi + \frac{w_0^2}{2}u_z - \frac{\partial^2\Phi}{\partial t^2} &= 0. \end{aligned} \tag{54}$$

The constitutive equations (Eq. (3)) in terms of potentials can be written as

$$\begin{aligned}
\sigma_{xz} &= (\mu+\kappa)\frac{\partial u_z}{\partial x} + \kappa\left(\frac{\partial \xi}{\partial y} - \frac{\partial \Phi}{\partial x}\right),\\
\sigma_{yz} &= (\mu+\kappa)\frac{\partial u_z}{\partial y} - \kappa\left(\frac{\partial \xi}{\partial x} + \frac{\partial \Phi}{\partial y}\right),\\
\sigma_{zx} &= \mu\frac{\partial u_z}{\partial x} - \kappa\left(\frac{\partial \xi}{\partial y} - \frac{\partial \Phi}{\partial x}\right),\\
\sigma_{zy} &= \mu\frac{\partial u_z}{\partial y} + \kappa\left(\frac{\partial \xi}{\partial x} + \frac{\partial \Phi}{\partial y}\right),\\
m_{xx} &= \alpha\nabla^2\xi + (\beta+\gamma)\left(\frac{\partial^2 \xi}{\partial x^2} + \frac{\partial^2 \Phi}{\partial x \partial y}\right),\\
m_{yy} &= \alpha\nabla^2\xi + (\beta+\gamma)\left(\frac{\partial^2 \xi}{\partial y^2} - \frac{\partial^2 \Phi}{\partial x \partial y}\right),\\
m_{yx} &= (\beta+\gamma)\frac{\partial^2 \xi}{\partial x \partial y} + \beta\frac{\partial^2 \Phi}{\partial y^2} - \gamma\frac{\partial^2 \Phi}{\partial x^2},\\
m_{xy} &= (\beta+\gamma)\frac{\partial^2 \xi}{\partial x \partial y} - \beta\frac{\partial^2 \Phi}{\partial x^2} + \gamma\frac{\partial^2 \Phi}{\partial y^2},
\end{aligned} \tag{55}$$

The buried sources inside the medium can be effectively treated as stress discontinuities across the plane $y = y_0$. The three loading cases considered in this study are shown in Fig. 2(a)–(c). The magnitude of these three loads acting on the line $y = y_0$ are $\exp[-i(kx + \omega t)]$ per unit area. These can be expressed as

$$m_{yy}(x, y = y_0^+, t) - m_{yy}(x, y = y_0^-, t) = \exp[-i(kx + \omega t)], \tag{56}$$

$$m_{yx}(x, y = y_0^+, t) - m_{yx}(x, y = y_0^-, t) = \exp[-i(kx + \omega t)], \tag{57}$$

$$\sigma_{yz}(x, y = y_0^+, t) - \sigma_{yz}(x, y = y_0^-, t) = \exp[-i(kx + \omega t)]. \tag{58}$$

The displacements and micro-rotations are required to be continuous across the plane $y = y_0$. These are given as

$$\phi_x(x, y = y_0^+, t) = \phi_x(x, y = y_0^-, t), \tag{59}$$

$$\phi_y(x, y = y_0^+, t) = \phi_y(x, y = y_0^-, t), \tag{60}$$

$$u_z(x, y = y_0^+, t) = u_z(x, y = y_0^-, t), \tag{61}$$

boundary conditions in a half-space are given by the vanishing of stresses at the free surface which is

$$m_{yy}(x, 0, t) = m_{yx}(x, 0, t) = \sigma_{yz}(x, 0, t) = 0. \tag{62}$$

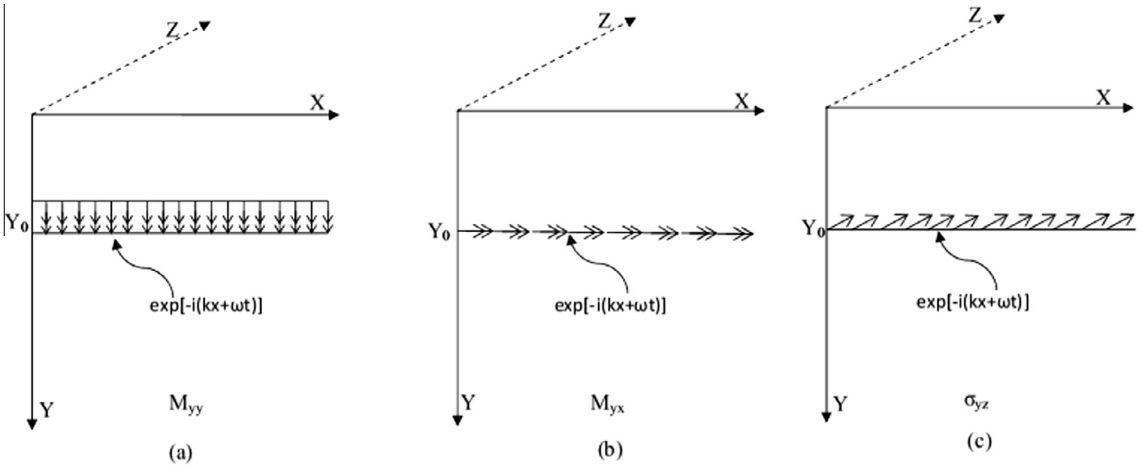

Fig. 2. (a)–(c) Three loading conditions for anti-plane strain problem.

The solutions of Eq. (54) can be written as

$$\begin{aligned}\xi(x,y,t) &= \tilde{\xi}(y)\exp[-i(kx+\omega t)],\\ \Phi(x,y,t) &= \tilde{\Phi}(y)\exp[-i(kx+\omega t)],\\ u_z(x,y,t) &= \tilde{u}_z(y)\exp[-i(kx+\omega t)].\end{aligned} \tag{63}$$

Here k is the real wave number along the x direction and ω stands for frequency. Substituting the above equation in Eq. (54), the governing equations can be rewritten as

$$\begin{aligned}&\frac{d^2\tilde{\xi}}{dy^2}+\left(\frac{\omega^2}{c_3^2}-\frac{w_0^2}{c_3^2}-k^2\right)\tilde{\xi}=0,\\ &\frac{d^2\tilde{u}_z}{dy^2}+\left(\frac{\omega^2}{c_2^2}-k^2\right)\tilde{u}_z-\mathrm{J}\frac{w_0^2}{2c_2^2}\frac{d^2\tilde{\Phi}}{dy^2}+\mathrm{J}\frac{k^2w_0^2}{2c_2^2}\tilde{\Phi}=0,\\ &\frac{d^2\tilde{\Phi}}{dy^2}+\left(\frac{\omega^2}{c_4^2}-\frac{w_0^2}{c_4^2}-k^2\right)\tilde{\Phi}+\frac{w_0^2}{2c_4^2}\tilde{u}_z=0.\end{aligned} \tag{64}$$

In region **I**, the solution to the equation can be expressed as

$$\begin{aligned}\tilde{\xi}(y) &= A^{\mathrm{I}}e^{-iv_0(y-y_0)}+B^{\mathrm{I}}e^{iv_0(y-y_0)},\\ \tilde{\Phi}(y) &= D_1^{\mathrm{I}}e^{-iv_1(y-y_0)}+D_2^{\mathrm{I}}e^{-iv_2(y-y_0)}+D_3^{\mathrm{I}}e^{iv_1(y-y_0)}+D_4^{\mathrm{I}}e^{iv_2(y-y_0)},\\ \tilde{u}_z(y) &= \varsigma_1\left(D_1^{\mathrm{I}}e^{-iv_1(y-y_0)}+D_3^{\mathrm{I}}e^{iv_1(y-y_0)}\right)+\varsigma_2\left(D_2^{\mathrm{I}}e^{-iv_2(y-y_0)}+D_4^{\mathrm{I}}e^{iv_2(y-y_0)}\right).\end{aligned} \tag{65}$$

In region **II**, the solution to the equation can be expressed as

$$\begin{aligned}\tilde{\xi}(y) &= A^{\mathrm{II}}e^{-iv_0(y-y_0)},\\ \tilde{\Phi}(y) &= D_1^{\mathrm{II}}e^{-iv_1(y-y_0)}+D_2^{\mathrm{II}}e^{-iv_2(y-y_0)},\\ \tilde{u}_z(y) &= \varsigma_1D_1^{\mathrm{II}}e^{-iv_1(y-y_0)}+\varsigma_2D_2^{\mathrm{II}}e^{-iv_2(y-y_0)},\end{aligned} \tag{66}$$

where

$$\varsigma_1=\frac{2c_4^2}{w_0^2}\left(k^2+v_1^2+\frac{w_0^2}{c_4^2}-\frac{\omega^2}{c_4^2}\right),$$

$$\varsigma_2=\frac{2c_4^2}{w_0^2}\left(k^2+v_2^2+\frac{w_0^2}{c_4^2}-\frac{\omega^2}{c_4^2}\right).$$

v_0, v_1 and v_2 are the vertical wave numbers defined through,

$$\begin{aligned}&v_0=\sqrt{\frac{\omega^2}{c_3^2}-\frac{w_0^2}{c_3^2}-k^2},\quad v_1=\sqrt{a_1-k^2},\quad v_2=\sqrt{a_2-k^2},\\ &a_{1,2}=\frac{(c_2^2+c_4^2)\omega^2}{2c_2^2c_4^2}+\frac{(w_0^2\mathrm{J}-4c_2^2)w_0^2}{8c_2^2c_4^2}\pm\sqrt{\frac{(c_2^2-c_4^2)^2}{4c_2^4c_4^4}\omega^4+\frac{w_0^2(w_0^2\mathrm{J}(c_2^2+c_4^2)-4c_2^2(c_2^2-c_4^2))}{8c_2^4c_4^4}\omega^2+\frac{w_0^4(w_0^2\mathrm{J}-4c_2^2)^2}{64c_2^4c_4^4}}.\end{aligned} \tag{67}$$

The total numbers of unknown coefficients are 9. These constants have to be found from the above nine boundary conditions. The stresses are zero along the free surface ($y=0$). From the Eq. (62) the constants $A^{\mathrm{I}}, D_1^{\mathrm{I}}$, and D_2^{I} can be expressed as

$$D_2^{\mathrm{I}}=\frac{1}{\Lambda_1\Lambda_4-\Lambda_2\Lambda_3}\left[\Lambda_6\Lambda_1\left(2kv_0(\beta+\gamma)e^{-iy_0(v_0+v_2)}B^{\mathrm{I}}-2(\beta v_1^2-\gamma k^2)e^{-iy_0(v_1+v_2)}D_3^{\mathrm{I}}\right)-(\Lambda_1\Lambda_5+\Lambda_2\Lambda_3)e^{-2iv_2y_0}D_4^{\mathrm{I}}\right], \tag{68}$$

$$D_1^{\mathrm{I}}=e^{-2iv_1y_0}D_3^{\mathrm{I}}+\frac{\Lambda_2}{\Lambda_1}\left[e^{-iy_0(v_1+v_2)}D_4^{\mathrm{I}}-e^{iy_0(v_2-v_1)}D_2^{\mathrm{I}}\right], \tag{69}$$

$$A^{\mathrm{I}}=-e^{-2iv_1y_0}B^{\mathrm{I}}+\frac{\left[\Lambda_7\left(e^{iy_0(v_1-v_0)}D_1^{\mathrm{I}}-e^{-iy_0(v_0+v_1)}D_3^{\mathrm{I}}\right)+\Lambda_8\left(e^{iy_0(v_2-v_0)}D_2^{\mathrm{I}}-e^{-iy_0(v_0+v_2)}D_4^{\mathrm{I}}\right)\right]}{\Lambda_5}. \tag{70}$$

The continuity of displacements and rotations along the plane $y=y_0$ (Eqs. (59)–(61)) results in

$$A^{\mathrm{II}}=A^{\mathrm{I}}+\frac{1}{\Lambda_{10}}\left[\Lambda_9B^{\mathrm{I}}-2kc_4^2(v_1+v_2)\left(v_1D_3^{\mathrm{I}}+v_2D_4^{\mathrm{I}}\right)\right], \tag{71}$$

$$D_1^{II} = D_1^I + \frac{1}{(v_1 - v_2)\Lambda_{10}}\left[(v_1 + v_2)\Lambda_{11}D_3^I + 2v_0\left(\omega^2 - w_0^2 - c_4^2(k^2 + v_2^2)\right)(kB^I - v_2 D_4^I)\right], \tag{72}$$

$$D_2^{II} = D_2^I + \frac{1}{(v_1 - v_2)\Lambda_{10}}\left[(v_1 + v_2)\Lambda_{12}D_4^I - 2v_0\left(\omega^2 - w_0^2 - c_4^2(k^2 + v_1^2)\right)\left(kB^I - v_1 D_3^I\right)\right], \tag{73}$$

where

$$\Lambda_1 = v_1\left[2(\mu+\kappa)\left((\alpha+\beta+\gamma)v_0^2 + \alpha k^2\right)\left(\omega^2 - w_0^2 - c_4^2(k^2+v_1^2)\right) + \kappa(\alpha+\beta+\gamma)w_0^2(k^2+v_0^2)\right],$$

$$\Lambda_2 = v_2\left[2(\mu+\kappa)\left((\alpha+\beta+\gamma)v_0^2 + \alpha k^2\right)\left(\omega^2 - w_0^2 - c_4^2(k^2+v_2^2)\right) + \kappa(\alpha+\beta+\gamma)w_0^2(k^2+v_0^2)\right],$$

$$\Lambda_3 = \left((\alpha+\beta+\gamma)v_0^2 + \alpha k^2\right)\left(\beta v_1^2 - \gamma k^2\right) + v_0 v_1 k^2(\beta+\gamma)^2,$$

$$\Lambda_4 = \left((\alpha+\beta+\gamma)v_0^2 + \alpha k^2\right)\left(\beta v_2^2 - \gamma k^2\right) + v_0 v_2 k^2(\beta+\gamma)^2,$$

$$\Lambda_5 = \left((\alpha+\beta+\gamma)v_0^2 + \alpha k^2\right)\left(\beta v_2^2 - \gamma k^2\right) - v_0 v_2 k^2(\beta+\gamma)^2,$$

$$\Lambda_6 = \left((\alpha+\beta+\gamma)v_0^2 + \alpha k^2\right),$$

$$\Lambda_7 = k v_1(\beta+\gamma),$$

$$\Lambda_8 = k v_2(\beta+\gamma),$$

$$\Lambda_9 = k^2 c_4^2(v_1+v_2) - v_0(\omega^2 - w_0^2 - c_4^2(k^2 - v_1 v_2)),$$

$$\Lambda_{10} = k^2 c_4^2(v_1+v_2) + v_0\left(\omega^2 - w_0^2 - c_4^2(k^2 - v_1 v_2)\right),$$

$$\Lambda_{11} = k^2 c_4^2(v_1-v_2) - v_0(\omega^2 - w_0^2 - c_4^2(k^2 + v_1 v_2)),$$

$$\Lambda_{12} = k^2 c_4^2(v_1-v_2) + v_0\left(\omega^2 - w_0^2 - c_4^2(k^2 + v_1 v_2)\right).$$

Six coefficients $\left(A^I, D_1^I, D_2^I, A^{II}, D_1^{II} \text{ and } D_2^{II}\right)$ are expressed in terms of other three coefficients $\left(B^I, D_3^I, \text{ and } D_4^I\right)$ in above equations (Eqs. (68)–(73)). These three coefficients have to be estimated by using the stress discontinuity condition along the plane $y = y_0$ (Eqs. (56)–(58)).

4.2.1. Results for specific source distributions

Loading case I:

$$m_{yy}(x, y = y_0^+, t) - m_{yy}(x, y = y_0^-, t) = 0,$$

$$m_{yx}(x, y = y_0^+, t) - m_{yx}(x, y = y_0^-, t) = 0,$$

$$\sigma_{yz}(x, y = y_0^+, t) - \sigma_{yz}(x, y = y_0^-, t) = \exp\left[-i(kx + \omega t)\right],$$

$$B^I = 0, \tag{74}$$

$$D_3^I = \frac{iw_0^2}{4c_4^2 v_1(\mu+\kappa)(v_1^2 - v_2^2)}, \tag{75}$$

$$D_4^I = -\frac{iw_0^2}{4c_4^2 v_2(\mu+\kappa)(v_1^2 - v_2^2)}, \tag{76}$$

Loading case II:

$$m_{yy}(x, y = y_0^+, t) - m_{yy}(x, y = y_0^-, t) = 0,$$

$$m_{yx}(x, y = y_0^+, t) - m_{yx}(x, y = y_0^-, t) = \exp\left[-i(kx + \omega t)\right],$$

$$\sigma_{yz}(x, y = y_0^+, t) - \sigma_{yz}(x, y = y_0^-, t) = 0,$$

$$B^{\mathrm{I}} = \frac{kc_4^2}{2\beta v_0(w_0^2 - \omega^2)}, \tag{77}$$

$$D_3^{\mathrm{I}} = -\frac{(\omega^2 - w_0^2 - c_4^2(k^2 + v_2^2))}{2\beta(v_1^2 - v_2^2)(w_0^2 - \omega^2)}, \tag{78}$$

$$D_4^{\mathrm{I}} = \frac{(\omega^2 - w_0^2 - c_4^2(k^2 + v_1^2))}{2\beta(v_1^2 - v_2^2)(w_0^2 - \omega^2)}, \tag{79}$$

Loading case III:

$$m_{yy}(x, y = y_0^+, t) - m_{yy}(x, y = y_0^-, t) = \exp[-i(kx + \omega t)],$$

$$m_{yx}(x, y = y_0^+, t) - m_{yx}(x, y = y_0^-, t) = 0,$$

$$\sigma_{yz}(x, y = y_0^+, t) - \sigma_{yz}(x, y = y_0^-, t) = 0,$$

$$B^{\mathrm{I}} = \frac{1}{2(\alpha + \beta + \gamma)(k^2 + v_0^2)}, \tag{80}$$

$$D_3^{\mathrm{I}} = \frac{k\left(\omega^2 - w_0^2 - c_4^2(k^2 + v_2^2)\right)}{2v_1c_4^2(v_1^2 - v_2^2)(\alpha + \beta + \gamma)(k^2 + v_0^2)}, \tag{81}$$

$$D_4^{\mathrm{I}} = -\frac{k(\omega^2 - w_0^2 - c_4^2(k^2 + v_1^2))}{2v_2c_4^2(v_1^2 - v_2^2)(\alpha + \beta + \gamma)(k^2 + v_0^2)}. \tag{82}$$

The obtained solutions are valid for the loading cases shown in Fig. 2 where the loads act periodically all over the plane $y = y_0$ and harmonically in time. The corresponding solutions for the three unidirectional unit impulses can be obtained by using the Fourier integral representation of the Dirac delta function.

5. Reduced micropolar elastic half-space

The above derived expressions can be used to simulate Green's functions in a micropolar medium. The main limitation with the micropolar theory is that six material constants are required to simulate ground motion. These constants are not directly available for rock and soil medium. To circumvent these difficulties, Schwartz et al. [25] proposed reduced micropolar theory to model granular materials. In this theory, the material point in a continuum is defined by three displacements $\mathbf{u}$ and three rotations ϕ which are kinematically independent. In reduced micropolar theory the particles are free to rotate (micro rotation) but the continuum does not offer resistance to micro-rotation, unlike micropolar theory. The stress tensor is asymmetric and couple stress tensor is zero. By this assumption three micropolar constants (α, β, γ) are eliminated. Previously Grekova et al. [20] studied surface wave propagation in reduced Cosserat medium. The equations of the motions in terms of $\mathbf{u}$ and ϕ can be expressed as

$$\begin{aligned} &c_1^2\nabla\nabla\cdot\boldsymbol{u} - c_2^2\nabla\times\nabla\times\mathbf{u} + \frac{\mathrm{J}w_0^2}{2}\nabla\times\phi - \ddot{\mathbf{u}} = 0, \\ &\frac{w_0^2}{2}\nabla\times\mathbf{u} - w_0^2\boldsymbol{\phi} - \ddot{\boldsymbol{\phi}} = 0, \end{aligned} \tag{83}$$

where

$$c_1^2 = \frac{\lambda + 2\mu + \kappa}{\rho}, \quad c_2^2 = \frac{\mu + \kappa}{\rho}, \quad w_o^2 = \frac{2\kappa}{\rho J}. \tag{84}$$

5.1. Ground motion at free surface of half-space due to a buried source

5.1.1. Plane strain

For a plane strain problem, the displacement and rotation vector is represented as $\mathbf{u} = (u_x, u_y, 0)$ and $\phi = (0, 0, \phi_z)$. Two potential functions, q and Ψ, can be defined to describe the displacements in x- and y-directions.

$$u_x = \frac{\partial q}{\partial x} + \frac{\partial \Psi}{\partial y}, \quad u_y = \frac{\partial q}{\partial y} - \frac{\partial \Psi}{\partial x}, \quad \phi_z = \phi. \tag{85}$$

The equations of motion for plane deformation parallel to *xy* plane in terms of the potentials are

$$\begin{aligned} c_1^2\left(\frac{\partial^2 q}{\partial x^2}+\frac{\partial^2 q}{\partial y^2}\right)-\frac{\partial^2 q}{\partial t^2}=0,\\ c_2^2\left(\frac{\partial^2 \Psi}{\partial x^2}+\frac{\partial^2 \Psi}{\partial y^2}\right)+\frac{\mathrm{J}w_0^2}{2}\phi-\frac{\partial^2 \Psi}{\partial t^2}=0. \end{aligned} \tag{86}$$

The constitutive equations (Eq. (3)) in terms of potentials can be written as

$$\begin{aligned} \sigma_{xx}&=\lambda\nabla^2 q+(2\mu+\kappa)\left(\frac{\partial^2 q}{\partial x^2}+\frac{\partial^2 \Psi}{\partial x\partial y}\right),\\ \sigma_{yy}&=\lambda\nabla^2 q+(2\mu+\kappa)\left(\frac{\partial^2 q}{\partial y^2}-\frac{\partial^2 \Psi}{\partial x\partial y}\right),\\ \sigma_{xy}&=(2\mu+\kappa)\frac{\partial^2 \mathrm{q}}{\partial x\partial y}+\mu\frac{\partial^2 \Psi}{\partial y^2}-(\mu+\kappa)\frac{\partial^2 \Psi}{\partial x^2}-\kappa\phi,\\ \sigma_{yx}&=(2\mu+\kappa)\frac{\partial^2 \mathrm{q}}{\partial x\partial y}-\mu\frac{\partial^2 \Psi}{\partial x^2}+(\mu+\kappa)\frac{\partial^2 \Psi}{\partial y^2}+\kappa\phi. \end{aligned} \tag{87}$$

The buried sources inside the medium can be effectively treated as stress discontinuities across the plane $y = y_0$. The magnitude of these three loads acting on the line $y = y_0$ are $\exp[-i(kx + \omega t)]$ per unit area. These can be expressed as

$$\sigma_{yy}(x,y=y_0^+,t)-\sigma_{yy}(x,y=y_0^-,t)=\exp[-i(kx+\omega t)], \tag{88}$$

$$\sigma_{yx}(x,y=y_0^+,t)-\sigma_{yx}(x,y=y_0^-,t)=\exp[-i(kx+\omega t)]. \tag{89}$$

The displacements and micro-rotations are required to be continuous across the plane $y = y_0$. These are given as

$$u_x(x,y=y_0^+,t)=u_x(x,y=y_0^-,t), \tag{90}$$

$$u_y(x,y=y_0^+,t)=u_y(x,y=y_0^-,t). \tag{91}$$

The boundary conditions in a half-space are given by the vanishing of stresses at the free surface which is

$$\sigma_{yy}(x,0,t)=\sigma_{yx}(x,0,t)=0 \tag{92}$$

The solutions of Eq. (86) can be written as

$$\begin{aligned} q(x,y,t)&=\tilde{q}(y)\exp[-i(kx+\omega t)],\\ \Psi(x,y,t)&=\tilde{\Psi}(y)\exp[-i(kx+\omega t)],\\ \phi(x,y,t)&=\tilde{\phi}(y)\exp[-i(kx+\omega t)]. \end{aligned} \tag{93}$$

Here k is the real wave number along the x direction and ω stands for frequency. Substituting the above equation in Eq. (86), the governing equations can be rewritten as

$$\begin{aligned} \frac{d^2\tilde{q}}{dy^2}+\left(\frac{\omega^2}{c_1^2}-k^2\right)\tilde{q}=0,\\ \frac{d^2\tilde{\Psi}}{dy^2}+\left(\frac{\omega^2}{c_2^2}-k^2\right)\tilde{\Psi}+\mathrm{J}\frac{w_0^2}{2c_2^2}\tilde{\phi}=0. \end{aligned} \tag{94}$$

From Eq. (83b) $\tilde{\phi}$ can be expressed in terms of potential $\tilde{\Psi}$ as

$$\tilde{\phi}=\frac{w_0^2}{2(\omega^2-w_0^2)}\left[-k^2\tilde{\Psi}+\frac{d^2\tilde{\Psi}}{dy^2}\right]. \tag{95}$$

Substitute equation (95) in Eq. (94b) for $\tilde{\phi}$ and the solution to the Eq. (94) can be expressed as
In region I

$$\begin{aligned} \tilde{q}(y)&=A^{\mathrm{I}}e^{-i\nu_0(y-y_0)}+B^{\mathrm{I}}e^{i\nu_0(y-y_0)},\\ \tilde{\Psi}(y)&=D_1^{\mathrm{I}}e^{-i\nu_1(y-y_0)}+D_2^{\mathrm{I}}e^{i\nu_1(y-y_0)}. \end{aligned} \tag{96}$$

In region II

$$\begin{aligned} \tilde{q}(y)&=A^{\mathrm{II}}e^{-i\nu_0(y-y_0)},\\ \tilde{\Psi}(y)&=D_1^{\mathrm{II}}e^{-i\nu_1(y-y_0)}, \end{aligned} \tag{97}$$

where v_0, and v_1 are the vertical wave numbers defined through,

$$v_0 = \sqrt{\frac{\omega^2}{c_1^2} - k^2}; \quad v_1 = \sqrt{\frac{4(w_0^2 - \omega^2)\left(\omega^2 - k^2 c_2^2\right) + Jk^2 w_0^4}{4c_2^2(w_0^2 - \omega^2) - Jw_0^4}}. \tag{98}$$

Grekova et al. [20] studied wave propagation in isotropic reduced Cosserat half-space. $v_0 = 0$ and $v_1 = 0$ correspond to the dispersion relations for the compression and shear-rotational waves in the reduced Cosserat medium. The compression wave is similar to classical continuum. The shear wave is coupled with rotation wave and the phase velocity of the shear wave is function of frequency.

The total number of unknown coefficients is 6. These constants have to be found from the above six boundary conditions. The displacements are continuous along the plane ($y = y_0$). From the Eqs. (90) and Eq. (90).

$$D_1^{II} = \Gamma_3 B^I + D_1^I + \Gamma_1 D_2^I, \tag{99}$$

$$A^{II} = \Gamma_1 B^I + A^I - \Gamma_2 D_2^I. \tag{100}$$

The stresses are zero along the free surface ($y = 0$). From the Eq. (92).

$$A^I = (PP)B^I + (SP)D_2^I, \tag{101}$$

$$D_1^I = (PS)B^I + (SS)D_2^I, \tag{102}$$

where *PP*, *PS*, *SP* and *SS* are reflection coefficients. It can be shown that as $\kappa \to 0$, these reflection coefficients are as same as linear elastic reflection coefficients reported in Aki and Richards [26].where

$$PP = \frac{(\Gamma_5\Gamma_4 - \Gamma_6)e^{-2iy_0 v_0}}{\Gamma_5\Gamma_4 + \Gamma_6},$$

$$SP = \frac{2\Gamma_4\Gamma_6 e^{-iy_0(v_1+v_0)}}{\Gamma_5\Gamma_4 + \Gamma_6},$$

$$PS = -\frac{2\Gamma_5 e^{-iy_0(v_1+v_0)}}{\Gamma_5\Gamma_4 + \Gamma_6},$$

$$SS = \frac{(\Gamma_5\Gamma_4 - \Gamma_6)e^{-2iy_0 v_1}}{\Gamma_5\Gamma_4 + \Gamma_6},$$

$$\Gamma_1 = \frac{k^2 - v_0 v_1}{k^2 + v_0 v_1},$$

$$\Gamma_2 = \frac{2kv_1}{k^2 + v_0 v_1},$$

$$\Gamma_3 = \frac{2kv_0}{k^2 + v_0 v_1},$$

$$\Gamma_4 = \frac{(2\mu + \kappa)kv_1}{\lambda(k^2 + v_0^2) + v_0^2(2\mu + \kappa)},$$

$$\Gamma_5 = 2kv_0(2\mu + \kappa)(\omega^2 - w_0^2),$$

$$\Gamma_6 = 2\mu(k^2 - v_1^2)(w_0^2 - \omega^2) + \kappa(2v_1^2\omega^2 + w_0^2(k^2 - v_1^2)).$$

Results for specific source distributions

Loading case I:

$$\sigma_{yy}(x, y = y_0^+, t) - \sigma_{yy}(x, y = y_0^-, t) = 0,$$

$$\sigma_{yx}(x, y = y_0^+, t) - \sigma_{yx}(x, y = y_0^-, t) = \exp[-i(kx + \omega t)],$$

$$D_2^I = \frac{(\omega^2 - w_0^2)}{(k^2 + v_1^2)\left[2\mu(\omega^2 - w_0^2) + \kappa(2\omega^2 - w_0^2)\right]}, \tag{103}$$

$$B^{I} = -\frac{k(\omega^2 - w_0^2)}{v_0(k^2 + v_1^2)\left[2\mu(\omega^2 - w_0^2) + \kappa(2\omega^2 - w_0^2)\right]}. \tag{104}$$

Loading case II:

$$\sigma_{yy}(x, y = y_0^+, t) - \sigma_{yy}(x, y = y_0^-, t) = \exp[-i(kx + \omega t)],$$

$$\sigma_{yx}(x, y = y_0^+, t) - \sigma_{yx}(x, y = y_0^-, t) = 0,$$

$$D_2^{I} = \frac{k}{2v_1(\lambda + 2\mu + \kappa)(k^2 + v_0^2)}, \tag{105}$$

$$B^{I} = \frac{1}{2(\lambda + 2\mu + \kappa)(k^2 + v_0^2)}. \tag{106}$$

The obtained solutions are valid for the loading cases shown in Fig. 1(a) and (b) where the loads act periodically all over the plane $y = y_0$ and harmonically in time. The corresponding solutions for the two unidirectional unit impulses can be obtained by using the Fourier integral representation of the Dirac delta function.

5.1.2. Anti-plane strain

For a anti-plane strain problem, the displacement and rotation vector is represented as $\mathbf{u} = (0, 0, u_z)$ and $\boldsymbol{\phi} = (\phi_x, \phi_y, 0)$. The equations of motion for plane deformation parallel to xy plane

$$c_2^2\left(\frac{\partial^2 u_z}{\partial x^2} + \frac{\partial^2 u_z}{\partial y^2}\right) + \frac{Jw_0^2}{2}\left(\frac{\partial \phi_y}{\partial x} - \frac{\partial \phi_x}{\partial y}\right) - \frac{\partial^2 u_z}{\partial t^2} = 0. \tag{107}$$

The constitutive equations (Eq. (3a)) in terms of displacements can be written as

$$\sigma_{yz} = (\mu + \kappa)\frac{\partial u_z}{\partial y} - \kappa\phi_x. \tag{108}$$

The buried sources inside the medium can be effectively treated as stress discontinuities across the plane $y = y_0$. The magnitude of the load acting on the line $y = y_0$ is $\exp[-i(kx + \omega t)]$ per unit area. This can be expressed as

$$\sigma_{yz}(x, y = y_0^+, t) - \sigma_{yz}(x, y = y_0^-, t) = \exp[-i(kx + \omega t)]. \tag{109}$$

The displacement is required to be continuous across the plane $y = y_0$. These are given as

$$u_z(x, y = y_0^+, t) = u_z(x, y = y_0^-, t). \tag{110}$$

The boundary conditions in a half-space are given by the vanishing of stresses at the free surface which is

$$\sigma_{yz}(x, 0, t) = 0. \tag{111}$$

The solution of Eq. (107) can be written as

$$\begin{aligned} \phi_x(x, y, t) &= \tilde{\phi}_x(y)\exp[-i(kx + \omega t)], \\ \phi_y(x, y, t) &= \tilde{\phi}_y(y)\exp[-i(kx + \omega t)], \\ u_z(x, y, t) &= \tilde{u}_z(y)\exp[-i(kx + \omega t)]. \end{aligned} \tag{112}$$

Here k is the real wave number along the x direction and ω stands for frequency. Substituting the above equation in Eq. (107), the governing equation can be rewritten as

$$c_2^2\frac{d^2\tilde{u}_z}{dy^2} + \frac{Jw_0^2}{2}\left(-ik\tilde{\phi}_y - \frac{\partial\tilde{\phi}_x}{\partial y}\right) + (\omega^2 - k^2c_2^2)\tilde{u}_z = 0. \tag{113}$$

From Eq. (83b) $\tilde{\phi}_x$ and $\tilde{\phi}_y$ can be expressed in terms of potential $\tilde{u}_z$ as

$$\begin{aligned} \tilde{\phi}_x &= \frac{w_0^2}{2(w_0^2 - \omega^2)}\frac{\partial\tilde{u}_z}{\partial y}, \\ \tilde{\phi}_y &= \frac{ikw_0^2}{2(w_0^2 - \omega^2)}\tilde{u}_z. \end{aligned} \tag{114}$$

Substitute equation (114) in Eq. (113), after rearranging (113)

$$\frac{d^2\tilde{u}_z}{dy^2} + v_0^2\tilde{u}_z = 0, \tag{115}$$

where

$$v_0 = \sqrt{\frac{4(\omega^2 - k^2c_2^2)(w_0^2 - \omega^2) + Jw_0^4}{4c_2^2(w_0^2 - \omega^2) - Jw_0^4}}.$$

In region I, the solution to the eq. can be expressed as

$$\tilde{u}_z(y) = A^{\mathrm{I}}e^{-iv_0(y-y_0)} + B^{\mathrm{I}}e^{iv_0(y-y_0)}. \tag{116}$$

In region II, the solution to the equation can be expressed as

$$\tilde{u}_z(y) = A^{\mathrm{II}}e^{-iv_0(y-y_0)}. \tag{117}$$

The total number of unknown coefficients is 3. These constants have to be found from the above three boundary conditions. Displacement is continuous along the plane ($y = y_0$). From Eq. (110).

$$A^{\mathrm{II}} = A^{\mathrm{I}} + B^{\mathrm{I}}. \tag{118}$$

The stress is zero along the free surface ($y = 0$). From Eq. (111), the constant A^I can be expressed as

$$A^{\mathrm{I}} = B^{\mathrm{I}}e^{-2iv_0y_0}. \tag{119}$$

Using the stress discontinuity boundary condition along the plane $y = y_0$ reported in Eq. (109), the constant B^I can be obtained as

$$B^{\mathrm{I}} = \frac{i}{2v_0\Lambda_1}, \tag{120}$$

where

$$\Lambda_1 = (\mu + \kappa) - \frac{\kappa w_0^2}{2(w_0^2 - \omega^2)},$$

As $\kappa \to 0$, it can be shown that these constants (B^I and A^I) are equivalent to linear elastic constants [26]. The obtained solutions are valid for the loading cases shown in Fig. 2c where the loads act periodically all over the plane $y = y_0$ and harmonically in time. The corresponding solutions for the unidirectional unit impulse can be obtained by using the Fourier integral representation of the Dirac delta function.

6. Numerical results

Ground motions have been simulated numerically to illustrate the application of derived analytical expressions. Time histories are estimated for anti-plane strain problem. Seven material constants (λ, μ, γ, α, β, j and κ) are required to define linear elastic micropolar material. Reduced micropolar theory requires two additional material constants κ and j in addition to Lame's constants (λ, μ). In the present study, the material properties (λ, μ, γ, and κ) are taken from the work of Eringen [24]. The following values of material parameters are used for numerical simulation, $\lambda = 7.59$ GPa, $\mu = 1.89$ GPa, $\gamma = 2.63$ kN, $\kappa = 0.015$ GPa, $\rho = 2180$ kg/mm^3 and $j = 0.196$ mm^2. The other two material constants α and β are approximately taken as γ. The response of micropolar elastic half space is estimated for three different loading cases shown in Fig. 2a. The response for unit impulsive sources as shown in Fig. 3 are obtained by taking Fourier transform.

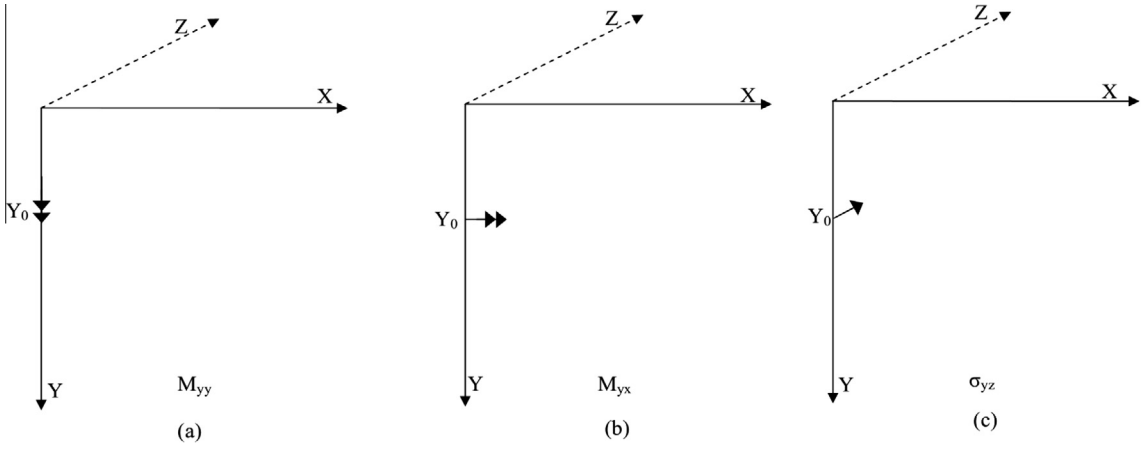

Fig. 3. (a)–(c) Three unit impulsive force/micro-moments applied at $(0, Y_0)$ corresponds to anti-plane strain problem.

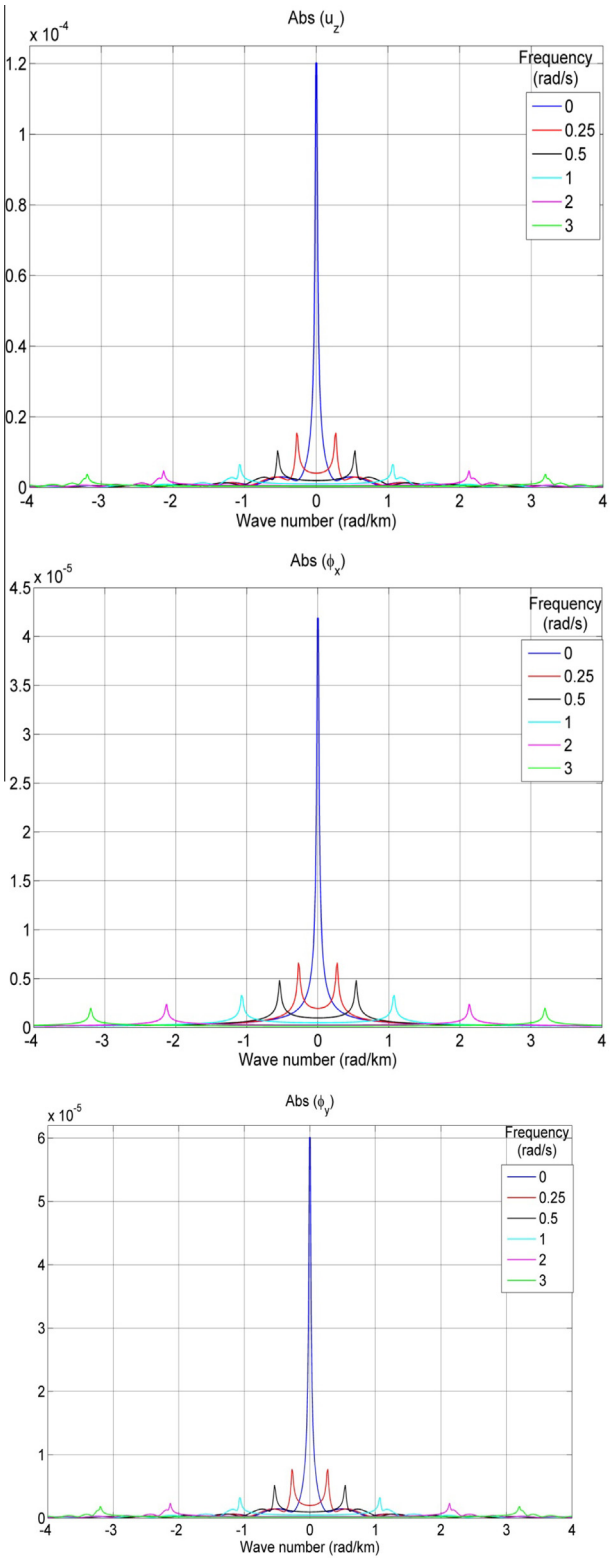

Fig. 4. Frequency-wavenumber spectra's of u_z, ϕ_x and ϕ_y.

$$G_z^p(x,y,t) = \frac{1}{2\pi}\int_{-\infty}^{\infty}\int_{-\infty}^{\infty} u_z(k,y,\omega)\exp[-i(kx+\omega t)]dkd\omega,$$
$$G_{\phi_x}^p(x,y,t) = \frac{1}{2\pi}\int_{-\infty}^{\infty}\int_{-\infty}^{\infty} \phi_x(k,y,\omega)\exp[-i(kx+\omega t)]dkd\omega, \quad (121)$$
$$G_{\phi_y}^p(x,y,t) = \frac{1}{2\pi}\int_{-\infty}^{\infty}\int_{-\infty}^{\infty} \phi_y(k,y,\omega)\exp[-i(kx+\omega t)]dkd\omega,$$

where $G_z^p, G_{\phi_x}^p$ and $G_{\phi_y}^p$ are the Green's functions of displacement u_z, rotation component ϕ_x and rotation component ϕ_y due to unit impulsive source applied in the p-direction. u_z, ϕ_x and ϕ_y are the response of the medium for loadings as shown in the Fig. 2. The infinite integrals in Eq. (121) can be numerically evaluated by discrete wave number method developed by Bouchon [27]. In this method, the infinite integrals are replaced by summations by introducing spatial periodicity in the loading. Selecting the appropriate cut-off frequency and wavenumber values is very important in discrete wave number method. These cut-off values should be selected such that no important information on displacement/rotation is left outside the integration limits. The cut-off values are selected from frequency (ω)-wavenumber (k) spectra's of u_z, ϕ_x and ϕ_y. The corresponding $\omega - k$ spectra's are plotted in Fig. 4. The cut-off frequency $\omega = 2$ rad/s and the cut-off wavenumber $k = 0.004$ rad/m. The final solution is obtained by Fourier transform in the complex frequency domain. A review of the discrete wave number method is available in Bouchon [27]. The ground motions are calculated at four locations on the free surface for a unit impulsive force/micro moment applied at a depth of 10 km (Y_0 = 10 km). The three constants B^I, D_3^I and D_4^I for unit impulsive force (F_{yz}) are estimated by using Eqs. (74)–(76), for all frequency (ω) and wavenumber (k) ranges. Other three constants A^I, D_1^I and D_2^I are calculated from Eqs. (68)–(70). The two potentials ξ, Φ and displacement u_z are estimated using Eqs. (65) and (63). The rotational components are obtained from potentials by using Eq. (53). These are substituted in Eq. (121) to obtain the displacement and rotation time histories for a unit impulsive force. The simulated time histories are shown in Fig. 5. In a similar fashion Green's functions are calculated for both unit impulsive micro-moment applied in x-direction (M_{yx}) and y-direction (M_{yy}) from Eq. (121) using the constants reported in Eqs. (77)–(79) and Eqs. (80)–(82). The simulated time histories at four locations on the surface of the half-space are reported in Figs. 6 and 7. From Figs. 5–7, it can be observed that the arrival time of the first wave increases with increase in the distance from the source. The peak values of the simulated displacements are higher than the amplitude of the micro-rotations for all the three loading cases. The unit impulsive micro-moment applied about x-axis (M_{yx}) has produced higher displacements and rotations compared to other two impulsive loads.

Fig. 8 shows the simulated displacement and rotation time histories for reduced micropolar elastic half-space. The two constants A^I and B^I are estimated by using Eqs. (119) and (120) for unit impulsive force for all frequency (ω) and wavenumber (k) ranges. The displacements and rotations are estimated from Eqs. (114) and (116). These are substituted in Eq. (112) and the Green's functions are simulated using Eq. (121). The obtained peak displacements and micro-rotations in a reduced micropolar half-space are lower than compared to micropolar half-space (Fig. 5). This can be attributed to the presence of additional microrotational waves in micropolar elastic half-space.

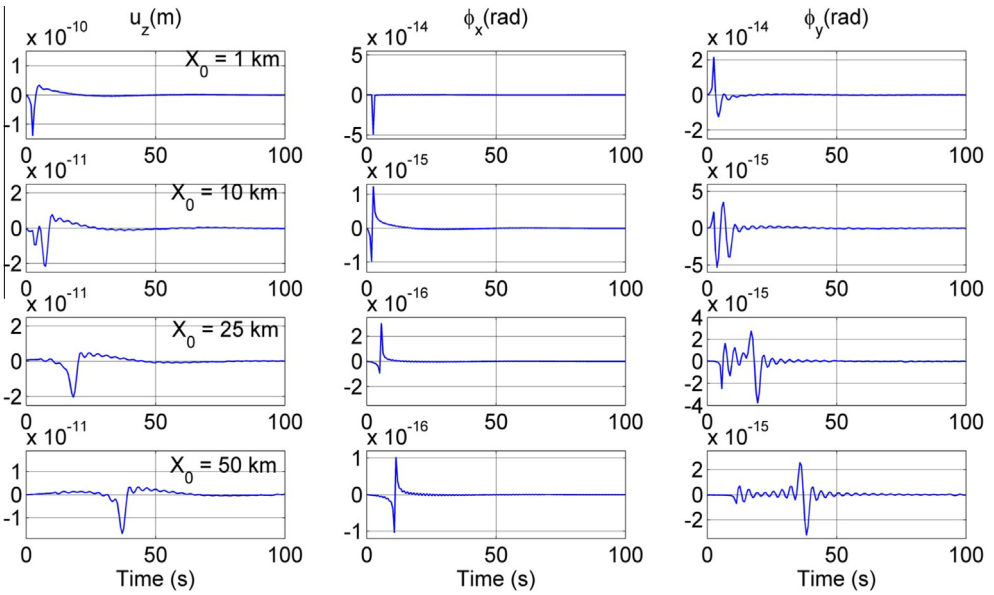

Fig. 5. Response of micropolar elastic half space for unit impulse force (F_{yz}).

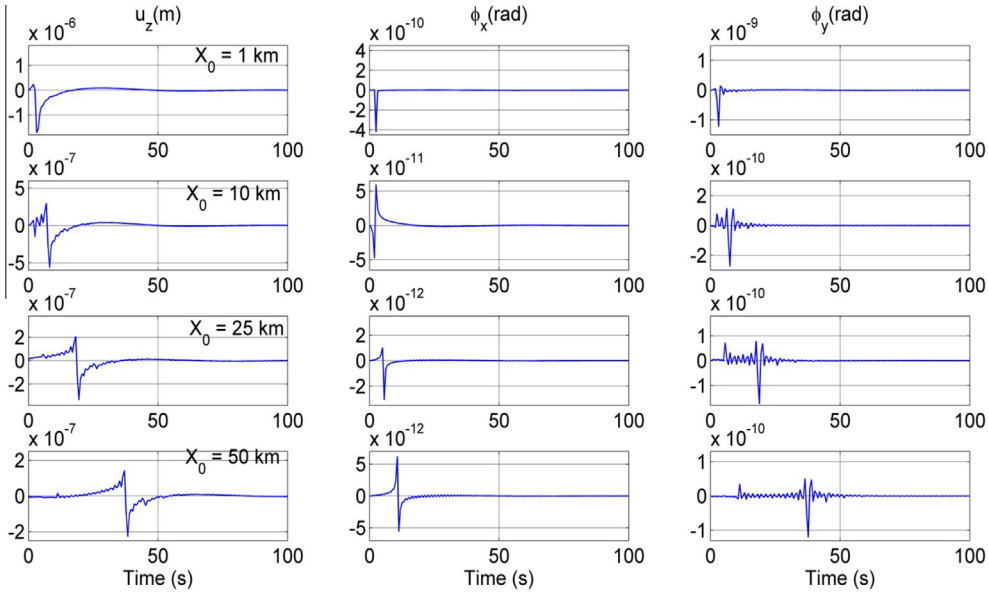

Fig. 6. Response of micropolar elastic half space for unit impulse micro-moment (M_{yx}).

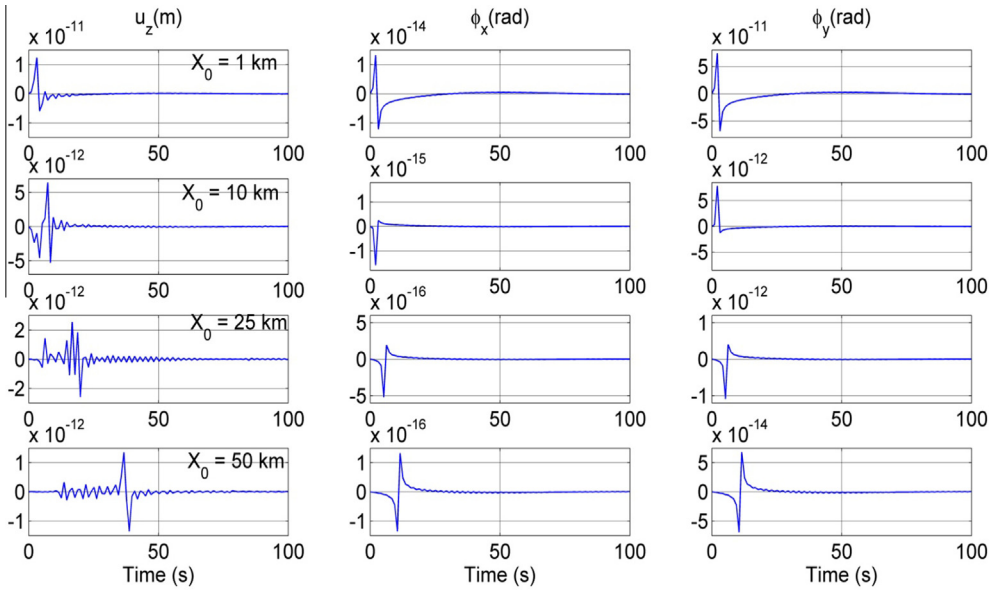

Fig. 7. Response of micropolar elastic half space for unit impulse micro-moment (M_{yy}).

It will be interesting here to compare the simulated displacements with linear elastic half-space solution available in Aki and Richards [26]. Accordingly the displacement (u_z) time history is simulated for an unit impulse force (F_{yz}) applied at a depth of 10 km (Y_0 = 10 km) for Reduced micropolar half space with $\kappa = 0$ (linear elastic half-space), Reduced micropolar half space and Micropolar half space. The material constants are kept same for all the four cases. The ground displacements are estimated at four locations on the surface of the half-space. Fig. 9 shows the comparison of displacement time histories for all the three mediums. The simulated displacement time history of reduced micropolar for $\kappa = 0$ is also valid for a linear elastic medium. The peak amplitude values for linear elastic and reduced micropolar elastic half space are close to each other. The micro effects on the simulated displacement time histories are more pronounced in the full micropolar medium compared to reduced micropolar medium. The peak displacement in a full micropolar elastic medium is also higher than compared to the reduced and linear elastic half-space.

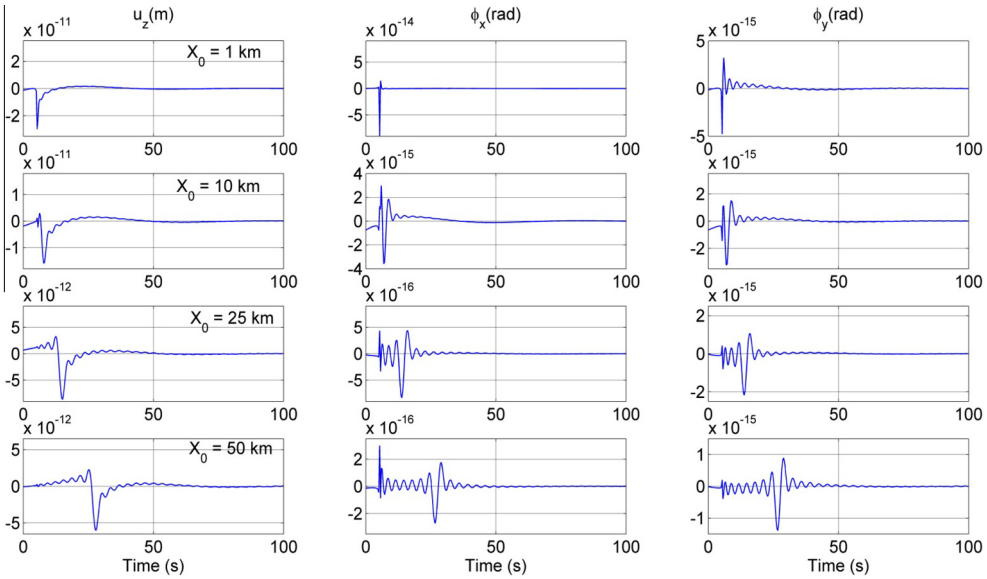

Fig. 8. Response of reduced micropolar elastic half space for unit impulse force (F_{yz}).

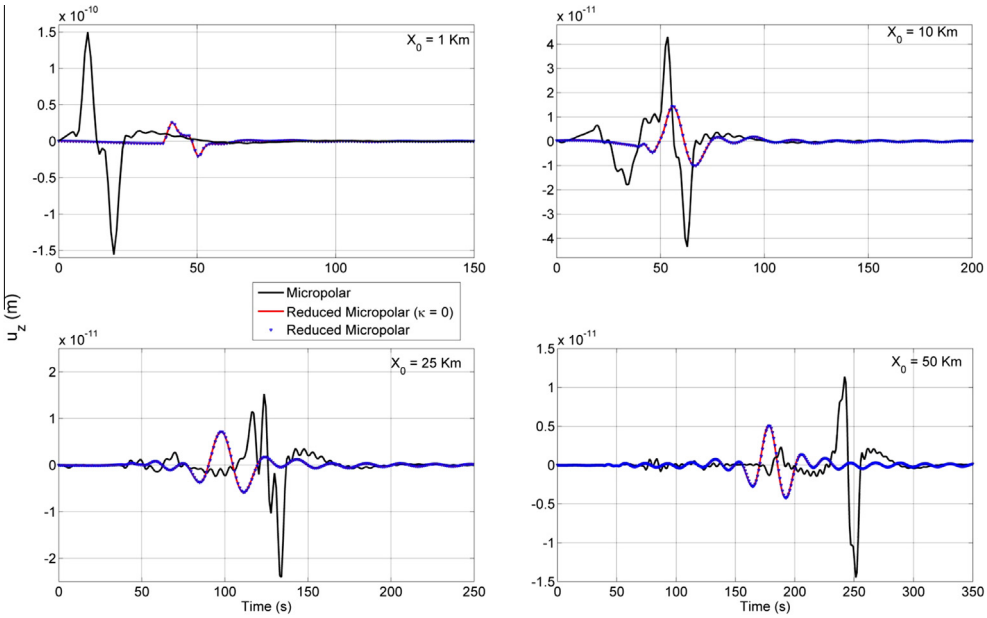

Fig. 9. Comparison of displacements for unit impulse force (F_{yz}).

In addition to Lame's constants only two additional material constants rotational inertia (j) and kappa (κ) are required to define reduced micropolar medium. In this present study $j = 0.196\text{e}{-6}\ \text{m}^2$ is used to simulate response of the reduced micropolar medium. For earth medium j value may be very high because of the presence of big stones, hard rocks and heterogeneity. Ground motions are simulated for four different values of j whose order varies from 10^{-6} to $10^4\ \text{m}^2$ to understand the effect of j on ground motions. The simulated ground motions are presented in Fig. 10. It can be observed form Fig. 10, that the effect of j on translation motion (u_z) is negligible. The rotational motions increase with increase in the rotational inertia of the medium. The effect of rotational inertia is observed only in rotational motions. The rotational inertia (j) and kappa (κ) values for reduced micropolar and additional three material constants (α, β and γ) for full micropolar earth medium can be estimated once sufficient recorded rotational ground motions data becomes available.

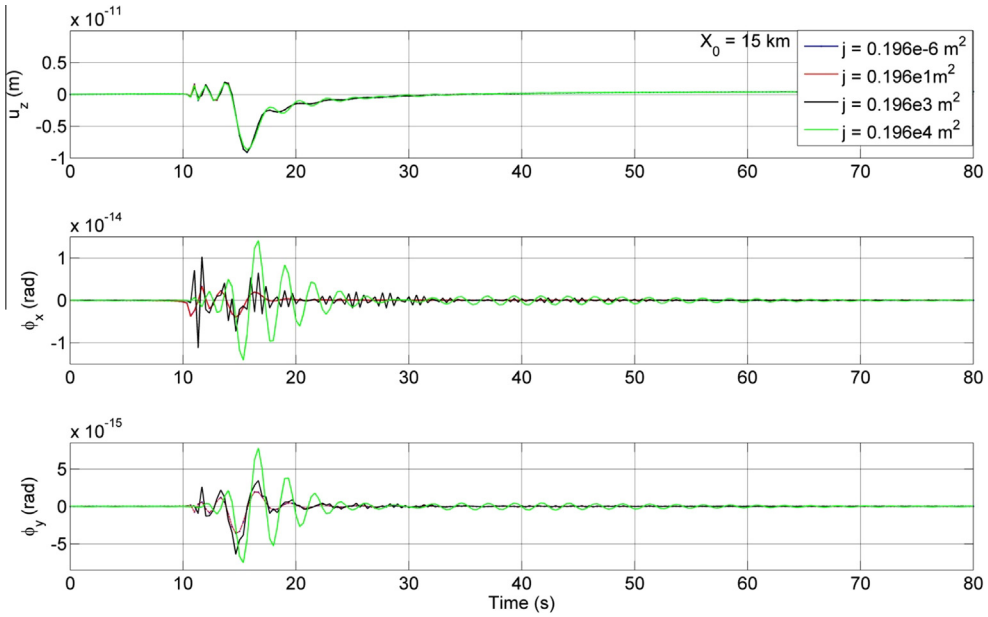

Fig. 10. Effect of rotational inertia (j) on ground motions.

7. Summary and conclusions

In this article fundamental solutions for both micropolar and reduced micropolar half space have been presented. The problem is divided into plane strain and anti-plane strain by assuming that the waves are traveling in XY plane only. Greens functions for buried concentrated force and micro-moment have been derived. Fourier integral representation is used to derive the fundamental solutions. In addition to longitudinal and shear waves, micro-rotational waves are been observed in micropolar theory. A total of six material constants are required to fully define an elastic micropolar medium. For reduced micropolar half-space the number of constants required to define the medium is three. Given these material constants one can simulate translation and micro-rotation time histories for a given unit impulse force and micro-moment. The derived analytical expressions can be used to simulate displacement field at the ground surface due to an earthquake with known rupture characteristics. The earthquake sources are generally modeled as a moment tensors. The advantage with micropolar theory is that one can apply directly the impulsive micro-moments in the half space. This theory can be used to simulate both rotational and translation ground motions for earthquakes. Discrete wave number method can be used to numerically evaluate the infinite integrals (Eq. (121)) for estimating displacement and rotation time histories. The closed form analytical expressions of frequency wave number spectra obtained in this study can be directly used to understand the temporal and spatial variability of seismic ground motion. The corresponding correlation characteristics of ground motions can be estimated from the frequency wave number spectrum. Numerical results have been presented for anti-plane strain case. The displacement and rotational time histories due to a unit impulsive force and micro-moment are simulated for both reduced and full micropolar medium (Figs. 5–8).

In the present study, expressions for surface displacement field have been derived using wave propagation in a single layered elastic half-space. These expressions can be further used to obtain Green's functions for layered half-space using propagator based formalism [6].

The major limitation with the micropolar theory is that additional material constants and rotational inertia of the medium are required to simulate ground motion. No studies have been done till date to estimate these constants for rock and soil medium. However with recent developments in strong motion instrumentation, it has become possible to measure rotational motions during the earthquake. With the help of strong motion data, one can estimate the micropolar material properties of the rock medium.

References

[1] H. Lamb, On the propagation of tremors over the surface of an elastic solid, Philos. Trans. R. Soc. 203 (1904) 1–42.
[2] M. Bouchon, A simple method to calculate Green's functions for elastic layered media, Bull. Seismol. Soc. Am. 71 (1981) 959–971.
[3] J.E. Luco, R.J. Apsel, On the Green's functions for a layered half-space. I, Bull. Seismol. Soc. Am. 73 (1983) 909–929.
[4] B. Chouet, Representation of an extended seismic source in a propagator-based formalism, Bull. Seismol. Soc. Am. 77 (1987) 14–27.
[5] R. Zhang, L. Zhang, M. Shinozuka, Seismic waves in a laterally inhomogeneous layered medium. I: theory, J. Appl. Mech. ASME 64 (1997) 50–58.
[6] S.T.G. Raghukanth, Source mechanism model for ground motion simulation, Appl. Math. Model. 32 (2008) 1417–1435.

[7] S.H. Hartzell, T.H. Heaton, Inversion of strong ground motion and teleseismic waveform data for the fault rupture history of the 1979 Imperial valley, California, earthquake, Bull. Seismol. Soc. Am. 73 (6) (1983) 1553–1583.
[8] S.T.G. RaghuKanth, R.N. Iyengar, Strong motion compatible source geometry, J. Geophys. Res. 113 (2008) B04309.
[9] R. Yamaguchi, T. Odaka, Field study of the Izu-Hanto-oki earthquake of 1974, Spec. Bull. Earthquake Res. Inst. Univ. Tokyo 14 (1974) 241–255.
[10] V.W. Lee, M.D. Trifunac, Rocking strong earthquake accelerations, Int. J. Soil Dyn. Earthq. Eng. 6 (2) (1987) 75–89.
[11] J.E. Luco, Torsional response of structures to obliquely incident seismic SH waves, Earthq. Eng. Struct. Dyn. 4 (1976) 207–219.
[12] M. Takeo, Ground rotational motions recorded in near-source region of earthquakes, Geophys. Res. Lett. 25 (1998) 789–792.
[13] H. Igel, U. Schreiber, A. Flaws, B. Schuberth, A. Velikoseltsev, A. Cochard, Rotational motions induced by the M8.1 Tokachi-oki earthquake, September 25, 2003, Geophys. Res. Lett. 32 (2005) L08309.
[14] W. Suryanto, H. Igel, J. Wassermann, A. Cochard, B. Schuberth, D. Vollmer, F. Scherbaum, U. Schreiber, A. Velikoseltsev, First comparison of array-derived rotational ground motions with direct ring laser measurements, Bull. Seismol. Soc. Am. 96 (6) (2006).
[15] M. Bouchon, K. Aki, Strain, tilt, and rotation associated with strong ground motion in the vicinity of earthquake faults, Bull. Seismol. Soc. Am. 72 (5) (1982) 1717–1730.
[16] A.C. Eringen, Linear theory of micropolar elasticity, J. Math. Mech. 15 (1966) 909–923.
[17] M.A. Kulesh, V.P. Matveenko, I.N. Shardakov, Construction and analysis of an analytical solution for the surface Rayleigh wave within the framework of the Cosserat continuum, J. Appl. Mech. Tech. Phys. 46 (2005) 556–563.
[18] M.A. Kulesh, V.P. Matveenko, I.N. Shardakov, Propagation of surface elastic waves in the Cosserat medium, Acoust. Phys. 52 (2006) 186–193.
[19] M. Kulesh, Waves in linear elastic media with microrotations, part 1: isotropic full cosserat model, Bull. Seismol. Soc. Am. 99 (2009) 1416–1422.
[20] E.F. Grekova, M.A. Kulesh, G.C. Herman, Waves in linear elastic media with microrotations, part 2: isotropic reduced cosserat model, Bull. Seismol. Soc. Am. 99 (2009) 1423–1428.
[21] A.C. Eringen, Linear theory of micropolar viscoelasticity, Int. J. Eng. Sci. 5 (1967) 191–204.
[22] C.B. Kafadar, A.C. Eringen, Micropolar media-I the classical theory, Int. J. Eng. Sci. 9 (1971) 271–305.
[23] V.R. Parfitt, A.C. Eringen, Reflection of plane waves from flat boundary of a micropolar elastic half-space, J. Acoust. Soc. Am. 45 (1969) 1258–1272.
[24] A.C. Eringen, Microcontinuum Field Theories: Foundations and Solids, vol. 487, Springer, New York, 1999.
[25] L.M. Schwartz, D.L. Johnson, S. Feng, Vibrational modes in granular materials, Phys. Rev. Lett. 52 (1984) 831–834.
[26] K. Aki, P.G. Richards, Quantitative Seismology: Theory and Methods, vol. I, WH Freeman, New York, 1980.
[27] M. Bouchon, A review of the discrete wave number method, J. Geophys. Res. 160 (2003).